ULTRASOUND-TRIGGERED NANO-FORMULATIONS FOR PREVENTION AND TARGETING OF BACTERIAL BIOFILMS

Kamila Ganiyeva

Bachelor of Engineering and Technology

Submitted in fulfillment of the requirements for the degree of

Master of Science In Chemistry

School of Sciences and Humanities

Department of Chemistry

Nazarbayev University

Supervisors: Prof Vesselin Paunov (NU Chemistry, Astana, Kazakhstan),

Prof Gleb Sukhorukov (QMUL, London, UK)

July 2023

Abstract

Prior to the antibiotic era, bacterial infections were the leading cause of death. Antibiotics were developed to cure a variety of ailments and saved many lives. However, due to overuse and inappropriate use of antibiotics, the emergence of bacterial resistance has expedited the so-called "post-antibiotic age." As a result, increasing death rates due to resistant bacterial infections a significant threat to public health and the world economies. The ability of many bacterial strains to form biofilms is the leading cause of the high viability and spread of the bacteria in tissues and chronic wounds. Modern antibiotics have shown low effectiveness due to the impenetrable bacteria extra polymer substance (EPS) of the biofilm. In the present thesis we explore a new strategy to target and prevent formation of drug-resistant bacterial biofilm infections. We developed study, novel shellac/enzyme nanoparticle formulations of three different enzymes (Alcalase, Savinase, Cellulase) and explored their ability to target biofilms of *S. epidermidis.* Our idea is based on preventing the premature release of the enzyme which can degrade the biofilm by depositing a silica shell over the nanocarrier particles that covers the surface of sterically stabilized shellac core with encapsulated enzyme which plays a role in the stimulus-triggered release of an active component to eradicate bacterial biofilms. We assessed the quality of the formed silica shells using dynamic light scattering, Transmission Electron Microscopy (TEM) and Energy-dispersive X-ray spectroscopy. TEM imaging allowed to assess the thickness of the silica shell. We tested both uncoated and silica coated shellac/enzyme nanoparticles in their effectiveness to degrade the bacterial biofilms. The most efficient nano-formulations were TEOS-coated Cellulase-loaded shellac nanoparticles which showed significant decrease in the residual biofilm biomass of *S. epidermidis* bacteria strain. We observed a significant increase of the enzyme release from silica-coated enzyme nanocarriers upon application of ultrasonic trigger, compared with non-coated enzyme nanocarrier. Most of the additional amount of enzyme was released during and very shortly after sonication. This demonstrated a successful ultrasonic trigger for the particles in the biofilm. We also evaluated the cytotoxicity of these formulations where the results indicated only a modest cytotoxicity on HeLa cell line which were used as a proxy for human cells. We also did the same encapsulation by using (3-Aminopropyl)triethoxysilane (APTES) which lead to similar results, but apparently higher cytotoxicity towards Hela cells. The developed silica-encapsulated enzyme nanocarriers have the potential to prevent and target bacterial biofilm by pretreating surfaces prone to bacterial biofilm infection and triggering the enzyme release by application of medical grade ultrasound. The treatment of chronic wounds with such silica shell-encapsulated enzyme-loaded nanoparticles could help develop more efficient ways of removal of bacterial biofilm by using non-invasive techniques to improve patient outcomes.

Acknowledgements

I would like to express my deepest and heartfelt gratitude to my family, friends, and lab mates for their support in words and action. In this lengthy and challenging path of researcher, you were my guiding lights.

Special thanks to my supervisor, Dr. Vesselin N. Paunov, who made me excel heights that I did not even dream of. It is an invaluable experience to work in your laboratory, and I am grateful for your patience and guidance. I wish you fruitful and successful research. I would like to express my gratitude to my co-supervisor Dr. Gleb B. Sukhorukov for his valuable recommendations and advice.

I want to thank my thesis reviewers, Dr. Ellina Mun and Dr. Timur Atabaev, for your thorough and critical feedback that you gave me, it helped me a lot to improve my thesis.

The biologists of our laboratory deserve special recognition, Dana Amangeldinova and Aruzhan Seidakhanova, for your collaboration, your professionalism beacons your paths. Thank you for the fruitful cooperation.

I would like to recognize my beloved cats, Luffy and Mimi. When I was stuck and disappointed with the results, your silly antics brightened my days.

I am forever grateful to each of you for your support, love, and belief in me. This Master thesis would not have been possible without you.

Originality Statement

I KAMILA GANIYEVA hereby solemnly declare that this dissertation presented to the Department of Chemistry, Nazarbayev University was done by me under the supervision and guidance of PROF. VESSELIN PAUNOV AND PROF. GLEB SUKHORUKOV and that this is the true representation of my own research findings. References and quotations made in this work have been given the due acknowledgement and that no part of this work has ever been submitted for the award of any degree in this University or elsewhere. Any contribution made to the research by others, with whom I have worked at NU or elsewhere is explicitly acknowledged in the thesis. I also declare that the intellectual content of this thesis is the product of my own work, except to the extent that assistance from others in the project's design and conception or in style, presentation and linguistic expression is acknowledged.

PROF. VESSELIN PAUNOV		8 July 2023
(SUPERVISOR)	SIGNATURE	DATE

PROF. GLEB SUKHORUKOV		11 July 2023
(CO-SUPERVISOR)	SIGNATURE	DATE

KAMILA GANIYEVA		6 July 2023
(STUDENT)	SIGNATURE	DATE

Table of Contents

List of Abbreviations & Symbols

NPs	nanoparticles
AMR	antimicrobial resistance
EPS	extracellular polymeric substance
DFUs	diabetic foot ulcers
US	ultrasonography
DNA	deoxyribonucleic acid
RNA	ribonucleic acid
P. aeruginosa	*Pseudomonas aeruginosa*
S. aureus	*Staphylococcus aureus*
S. epidermidis	*Staphylococcus epidermidis*
E. coli	*Escherichia coli*
E. faecalis	*Enterococcus faecalis*
NZM	nanozymes
ROS	reactive oxygen species
ODTAB	octadecyl trimethyl ammonium bromide
P407	Poloxamer 407
APTES	(3-Aminopropyl)triethoxysilane
TEOS	tetraethyl orthosilicate
PDT	photodynamic therapy
DLS	dynamic light scattering
TEM	Transmission Electron Microscopy
SEM	Scanning Electron Microscopy
EDS	Energy Dispersive Spectroscopy
FT-IR	Fourier Transform Infrared spectroscopy
EE	encapsulation efficiency
BSA	Bovine serum albumin
BA	Bradford assay
IEP	isoelectric point
CV	Crystal Violet
NB	Nutrient Broth

MTS	[3-(4,5-dimethylthiazol-2-yl)-5-(3-carboxymethoxyphenyl)-2-(4-sulfophenyl)-2H-tetrazolium]
DAPI	(4′,6-diamidino-2-phenylindole)
PI	propidium iodide

List of Figures

List of Schemes

1 Introduction

Before the discovery of antibiotics, bacterial infections were the leading cause of high mortality and a severe threat to human health. Since Fleming discovered penicillin in 1928, antibiotics have been developed to treat various ailments and have saved countless lives. However, due to their misuse, improper use in agriculture, and especially overprescription of antibiotics have expedited the so-called "post-antibiotic age". It led to the establishment of different mechanisms of bacterial resistance [1]. Antimicrobial resistance (AMR) is a consequence of the inherent resistance of bacteria and resistance due to the formation of biofilms on the surface of the infected area. Additionally, AMR is often described as the capability of bacteria to endure and survive while exposed to antimicrobial (including antibiotic) agents. Antimicrobial agents can be applied to microorganisms to lower their growth potential, obstruct their reproduction, or even eradicate them [2].

According to recent reports [3, 4], the global estimation is that approximately one billion people have acute and chronic wounds. It leads to a high death rate and bacterial infection that poses a severe risk to public health and the economy. For instance, The National Institute of Health accounted that biofilms comprise up to 80% of microbial infections. Financial expenses for wound care in 2014 were $2.8 billion, there is an increase of up to $3.5 billion in 2021. Therefore, the global agenda in healthcare is to address bacterial infections resistant to treatment [5, 6].

Treatment of chronic wounds remains challenging because chronic inflammation is hard to manage. One of the reasons is that bacterial biofilms are one of the most frequent causes of bacterial resistance. Bacteria have the ability to adapt while being exposed to different environments through natural selection and spontaneous mutations as well as horizontal gene transfer. When colonizing surfaces, bacteria produce an extracellular polymeric substance (EPS) that consists of different carbohydrates, proteins, and nucleic acids which envelops their

colony. Such microbial colony of bacteria, fungi, and other microorganisms that can adapt, interact, and proliferate is known as a biofilm [7, 8]. The biofilm is a three-dimensional network of microorganisms and EPS created over time due to adhesion and division. The bacterial biofilm matrix has been found not only to be a binding agent for the bacterium but also helps to resist their treatment with antibacterial agents [9].

Microbial colonies are substantially self-organized, involving interaction between cells. The common principle of formation of bacterial biofilm depends on environment of bacteria, substrates, moisture and availability of nutrients [10]. The development of biofilms is a process of multiple stages which is illustrated in Figure 1. Specifically, researchers indicate five distinct stages of the biofilm formation, both (i) reversible attachment and (ii) irreversible attachment, (iii) extracellular polymeric substances development, (iv) growth of biofilm and (v) detachment/propagation stage [11]. Firstly, in the stage of reversible initial attachment of free-floating planktonic cells connect to the area by means of hydrophobic properties. After that stage the process becomes irreversible and it creates extracellular polymeric substances (EPS) while supporting the cell in attachment to the surface [12, 13, 14]. At the fourth stage, cell division, adsorption, signaling between cells to produce the EPS and maturation occurs. In the last stage, there is a process of biofilm partial dispersal where the disbanded cells colonize new surfaces and substrates and then resume the process of further biofilm formation. Nevertheless, the regulation process varies for different kinds of bacteria, subsequently some of stages could be skipped or vice-versa, additional stages could appear. The complete process of development and maturation of bacterial biofilms was not completely studied and the interactions between different strains of bacterial are still poorly understood.

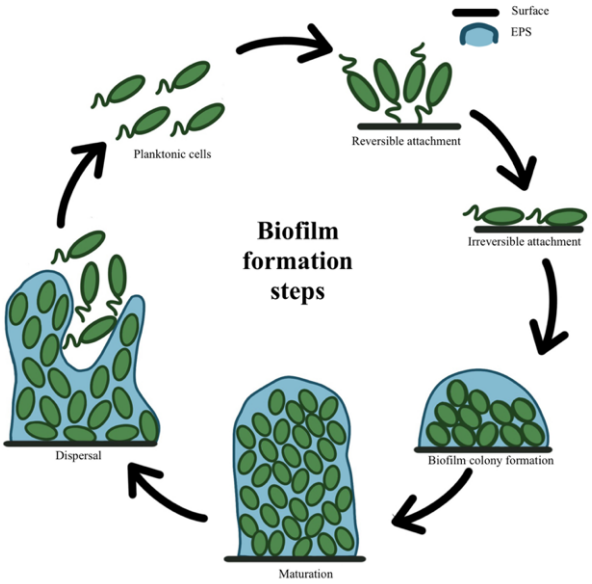

Figure 1. The process of biofilm formation.

Biofilms can delay healing and promote further infection and re-infection in wounds [15]. Additionally, biofilms formed on catheters and surgical implants may decrease the effectiveness of the treatment, rejection of the prosthesis, inflammation and swelling which necessitated implant removal and replacement. Chronic wounds are difficult to treat and susceptible to re-infection provide a great risk. They are more likely to develop arterial ulcers, venous leg ulcers, and diabetic foot ulcers (DFUs) which can progress into sepsis and lead to limb amputations and premature deaths.

The all bacteria despite their result on Gram evaluation have tendency to connect to the surface and create biofilms, the most widespread strains are *Staphylococcus aureus, Staphylococcus epidermidis* and *Pseudomonas aeruginosa* [15, 16, 17]. The study in 2018 revealed important statistics of cases with indwelling caused infection by staphylococcal species [15]. The quorum sensing mechanism has a great impact on density and signal transmission from cell to cell in biofilms. The process of connection of multiple cells is a sophisticated signaling mechanism for regulation of microbial cell density [18]. The autoinducers developed by cells and therefore the density property sequentially will be increased. The threshold of number of autoinducers correlates with cell density and eventually

will reach quorum level [19]. In this moment autoinducer will activate the repression mechanism. Generation of quorum sensing synthesize the common reaction which in time will regulate the size of biofilm and control virulence phenotypes [20]. The one united reaction provides the biofilm with advantageous properties of multicellular organism, which can adapt fast to the changes of conditions. Quantum sensing not only controls the population of cell but also communicates crucial mutations to the colony of biofilms and give accessible path to the nutrients and impacts on resistance to the antibiotics [21].

While states with progressive medicine achieved substantial success in treating chronic wounds, still part of their population suffers from chronic wounds. For instance, statistics show that nearly 5 million people in the United States are currently diagnosed with this condition [22]. As a therapeutic treatment in medicine, the most widely used method for preventing the development of bacterial biofilms is physical removal. It includes scrubbing of the wound surface, which causes negative effects such as extreme pain for the patient. Although in clinical trials, exfoliation of chronic wounds is primarily associated with a loss in wound surface area, the time required for treatment is often in the range of weeks to months and it has no significant correlation with full wound closure [23, 24]. In contrast to scrubbing, non-invasive approaches such as the application of ultrasound (US), as well as antibiotic and nanoparticles (NPs) therapies, are considered effective and promising methods for treating wounds [25, 26]. NPs can be composed based on biocompatible, biodegradable, non-toxic, and FDA-approved materials which are actually the most crucial factor in the development of such formulations. Additionally, Ag-Au nanocomposites, CuO NPs, $Mg(OH)_2$ NPs, silica NPs, and Au NPs have all demonstrated great effectiveness. However, due to the possibility of the establishment of hazardous chemicals as a result of poisonous, corrosive, and explosive precursors, it leads to the danger of their use for therapeutic purposes [27] and a low likelihood for FDA approval in clinical practice.

There is a rising awareness about side effects and potential problems with NPs-based antibacterial therapies as they can be cytotoxic to the surrounding healthy tissues and can contain persistent compounds. These toxic compounds remain within the NPs even in trace amounts and can cause undesirable effects [28]. One useful method for addressing this issue is use only green synthesis in producing NPs that are safe by design, without harmful residual compounds and high degradability post-use [29]. One of the crucial parts of the safe production is mutagenicity quality of nanomaterials. Another hidden issue is NPs and reactive oxygen species (ROS) side effect of impact on the DNA bacteria which may increase their mutagenicity. It is not well described issue should be presented more in the light of wide research on NPs. The threshold NPs concentration is the critical in this respect as weak treatments NPs at low concentration can improve the resistance of the biofilm. Therefore, accurate management of NPs-based treatment concentration is required since it could increase the mutagenicity in the biofilm [30]. Horizontal exchange of plasmids can contain genes useful for bacteria, such as genes for antibiotic resistance across different bacterial species in the biofilm colony. Moreover, the metal oxide-based NPs can also impact on formation of resistance in bacteria [28]. Therefore, future works should be focused on reasonable usage of NPs and their synthesis.

Alternative for the NPs consisting of metals, enzymatic debridement is a potential compromise to the damaged region to eliminate necrotic tissue and it is selective and effective for infected wounds. As a result of the enzymatic treatment, there is a chance to experience a stinging sensation and exudate [31]. The use of nanomaterials has immense promise for promoting self-healing processes that imitate regeneration. However, because damaged tissues are varied, a greater knowledge of the underlying processes and cellular cascades is required to tailor those nanomaterials for distinct wound healing applications.

Aims of the thesis

Present thesis aims to create core-shell type NPs consisting of shellac stabilized by a nonionic polymer having an enzyme encapsulated in the nanoparticle cores. For the enzyme to be encapsulated inside the particle, we produce a shell made of silica. After the preparation of core-shell NPs, ultrasound (US) is used to trigger the release of the active component, i.e., enzyme, which is released inside the EPS of the bacterial biofilm. Under the influence of US, the silica shell begins to gradually fracture, which increase its permeability with respect to the active component in the nanoparticle core. This allows the encapsulated enzyme to be released locally within the EPS of the biofilm which is degraded by enzymatic digestion and would facilitate its efficient removal from the substrate. This would be a particularly productive strategy as the surface of chronic wounds could be pretreated with such encapsulated enzyme carriers and their release activated by US only upon visible signs of infection. This would prevent the premature release of the enzyme and preserve their efficiency. These smart enzyme nanocarriers will be used to pre-treat the surface of various substrates which are prone to bacterial colonization resulting in the formation of a biofilm.

This method of treatment has advantages over the traditional ones, which includes a reduced risk of bleeding, and painful sensations during surgical removal of biofilms from chronic wounds. It is more effective due to the presence of an enzyme only within the biofilm which helps to dissolve the EPS when formed. Also, it provides direct targeting of the biofilms and the use of very small amounts of enzymes which avoids prolonged exposure to high enzyme concentration and undesired side effects due to their cytotoxicity to human cells.

2 Literature Review

Wounds are a vast group of damages that have variety of forms such as tiny cuts and scratches, wounds with varying degrees of severity and severe injury. Precisely, small wounds heal rapidly and without difficulties in healthy people. Contrariwise, there is a high probability of infection in larger wounds especially in old, immobile people. Moreover, in people who have diabetes, vascular disease, and cancer there is a delay of wound healing that is the main reason of formation of chronic ulcers, which can cause substantial discomfort, lengthy hospitalization, loss of function, and, in the worst-case scenario, amputations or the development of sepsis [32]. The intricacy of wound healing makes it difficult to reconstruct functioning skin after its formation. Figure 2 illustrates the differences between normal and chronic wounds.

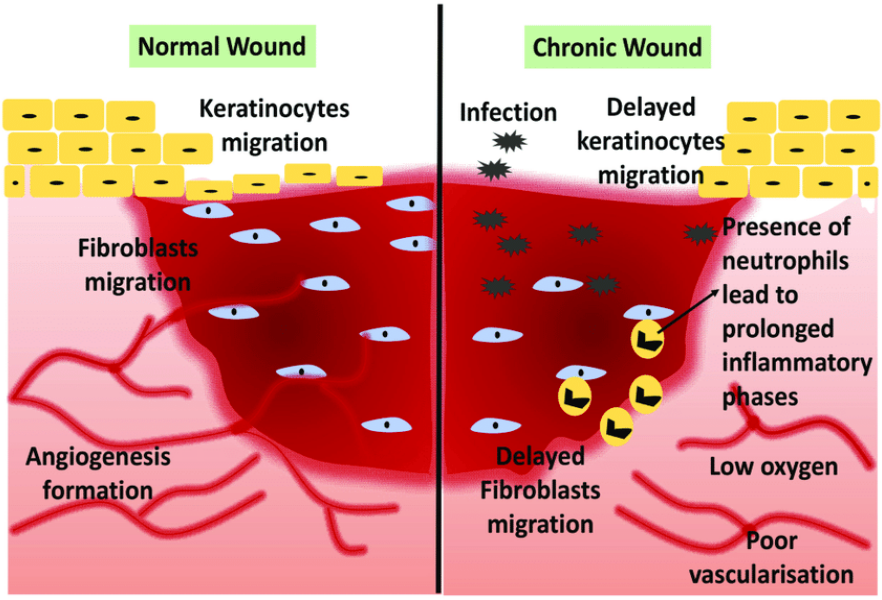

Figure 2. Comparison of normal and chronic wounds [32].

Physical removal, such as scrubbing and removal of the wound's upper layer, is the most clinically effective strategy for limiting the growth of bacterial biofilms. However, it is not an efficient, it is cumbersome, requires a qualified nurse or a surgeon, and is painful process for the patient. The clearing of the wound requires protracted observation for the reduction of

the wound area. Therefore, this therapy could take from weeks to months. Eventually, it does not guarantee the healing of the wound [33, 34]. Alternatively, non-invasive treatments for wound treatment, such as ultrasonography (US), antibiotics, and nanoparticle therapies, have shown promising.

One of the first research studies of application of US to treat chronic wounds dates back from 1994 and indicated high efficiency when coupled with the application of antibiotics. It has benefits, including deep tissue penetration, substantial focusing, and insignificant scattering of the infection. The US increased the EPS permeability and exposes the bacterial cell membrane to antibiotics [29] without breaking the biofilm. Nevertheless, the main drawback of this method is that it is a relatively new method and it has not undergone clinical testing [35]. The new wave of trials applied long treatment of wounds of 1 to 2 continuous days. This attempt is not feasible in reality and will not be practical due to economic and social reasons. The administration of the antibiotic to a specific area cannot be managed or regulated using this way of harnessing the synergistic association between US and antibiotic effectiveness. Therefore, scientists are cognizant of the harmful effects of antibiotics on the host microbiota and, as a result, an imbalance in bacteria [36].

One of the debatable problems is the application of antibiotics and antiseptics simultaneously due to malicious adverse reactions. The efficient extermination of infectious bacteria can be accomplished applying antibiotics in sufficient amounts [37]. This is frequently hampered by possible instability and due to it a quick decomposition. Furthermore, insufficient blood circulation limits the inflow of the antibiotics administered by oral intake or intravenously. Regarding the topical application of antibiotics, the most important is antimicrobial resistance caused by the EPS of the bacterial biofilm. It limits the penetration of the drug and it cannot reach the targeted site in therapeutic concentrations. In addition to

antimicrobial resistance, there are drawbacks such as superinfections, deferred hypersensitivity responses, and cytotoxicity.

The property of NPs to suppress biofilm growth has been investigated. Ag-Au nanocomposite particles, CuO NPs, $Mg(OH)_2$ NPs, silica NPs, and Au NPs have all shown outstanding performance in this area. Both Gram-positive and Gram-negative bacterial cells have negatively charged cell walls that can accumulate positively charged nanoparticles, which then electrostatically adhere to the cell membrane. Through alteration of cell permeability, nanoparticles can potentially eradicate the bacterial cell. NPs can penetrate bacterial cells due to their small size and intervene the synthesis of DNA, RNA, and proteins [38]. Biofilm synthesis was decreased by 25 and 30 per cent by AuNPs and AgNPs respectively. Biofilm generation was also reduced by 70–80 per cent due to the application of Au–Ag nanocomposites. The AgNPs and AuNPs can support the competitive intercalation of double-stranded genomic DNA in bacteria cells. The biofilm proportion was significantly dropped with subsequent rise of concentration of nanoparticles. Consequently, P. aeruginosa was successfully inhibited from building biofilms by AuNPs and AgNPs [39]. However, metallic NPs have side effects such as possibility of accumulation in parts of the body, cytotoxicity on the skin cells. Moreover, chemokine synthesis in macrophages is present when applying AgNPs [40]. In vitro studies show the toxicity of AgNPs which result in reduced healing process. Therefore, it is crucial to consider it when testing AgNPs in vivo.

Fe_3O_4, Fe_2O_3 nanozymes (NZM), AgNPs, and ZnO have been proposed as a treatment against biofilm development. Its properties are presented in Figure 3. However, there is a problem with the stability of prepared uncoated NZMs as they are unstable in physiological circumstances and therapeutic formulations, uncoated NZMs have drawbacks in clinical applications. The disadvantages such as ability to indiscriminately bind to biological tissues, harming healthy cells. To overcome this obstacle, a biocompatible coating is required to

improve their biocompatibility, enhance their penetration ability inside the biofilm, their catalytic activity, resulting in a more effective and targeted antibiofilm therapy [41].

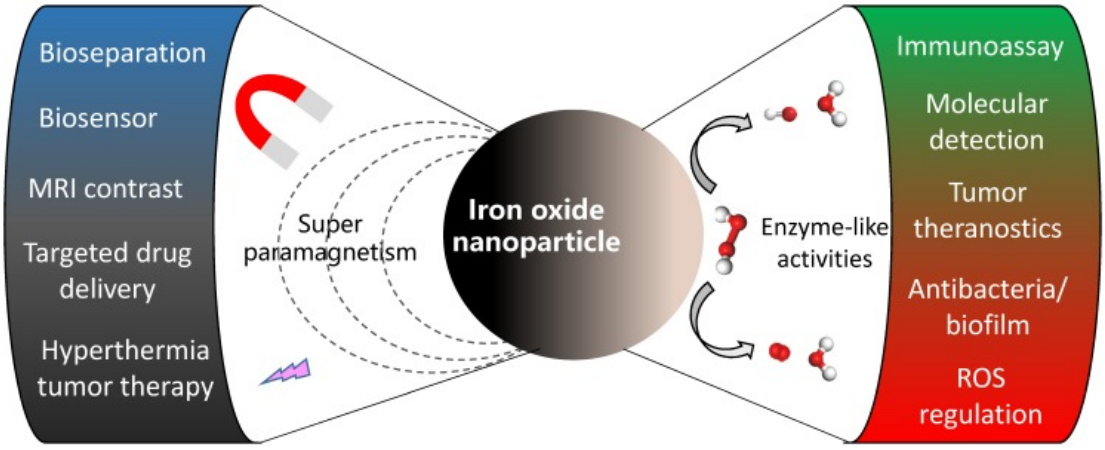

Figure 3. The novel iron oxide nanoparticles ' magnetic properties and enzyme-like activities [41].

An alternative solution consists of administering proteases from multiple sources (bacterial, vegetative, or animal) to remove necrotic tissue in the injured area on the surface of the skin. For infected wounds, enzymatic debridement is selective, efficient, and does not require any specialized tools or application methods. However, enzymatic treatment invokes a stinging sensation and exudate in the applied area [31]. Along with the previously researched approaches to treating chronic wounds, many techniques used modified implants, hydrogels, and nanotechnology inspired treatments. Because it combines biomechanical and pharmacological techniques, the multistage procedure with acoustically generated microbubbles and therapy by ultrasound of chronic wounds might be beneficial [42]. Hydrogels and implant prototypes, however, need more research to investigate how they interact with biofilms [43, 44].

Combining nanotechnology-based procedures within various fields of research may lead to more significant biofilm eradication and healing due to the stronger synergistic effects. It is important to consider the clinical applicability before making any investments in developing treatment solutions in any of these fields. On the other hand, recent developments

in biofilm research for implants and chronic wounds demonstrate a favorable trend that has the potential to improve patient comfort and health [31]. A more effective approach to this problem would be the cleverly reformulate of the treatments with the present antibiotics or enzymes with composite nano-formulations, which will prevent antimicrobial resistance.

Another research highlights the application of proteases that have been investigated for their ability to break up biofilms. Contrary to popular belief, bacteria are an important source of proteases to combat bacterial biofilms. Proteases have a significant advantage over other antibiofilm enzymes because they can hydrolyze EPS matrix proteins and adhesins, which allow a biofilm to adhere to a solid surface and bacteria to adhere to one another. It also degrades the EPS by enzymatic digestion of the glycoproteins which form the gel-like network of the biofilm matrix. The research study [45] reported on the use of both antibiotics and enzyme-functionalized nanoparticles. Scientists used Carbopol nanogel that has an antibiotic payload and a protease surface functionality. Cross-linked polymer chains in polyacrylic acid co-polymer nanogels have an anionic charge on their surface and inside due to the presence of ionizable COOH groups. These nanogel particles have shown to be effective in encasing cationic antibiotics while still being biocompatible. Additionally, cationic coatings on nanogels, such as poly (diallyldimethylammonium chloride) and branching polyethyleneimine [46, 47], can boost the effectiveness of antibiotics by concentrating the drug locally and preventing tissue damage while also targeting bacteria's anionic cell walls. On the other hand, the positive charge of the Alcalase enzyme at neutral pH helps to electrostatically attach this enzyme on the Carbopol nanogel surface, as shown in Scheme 1.

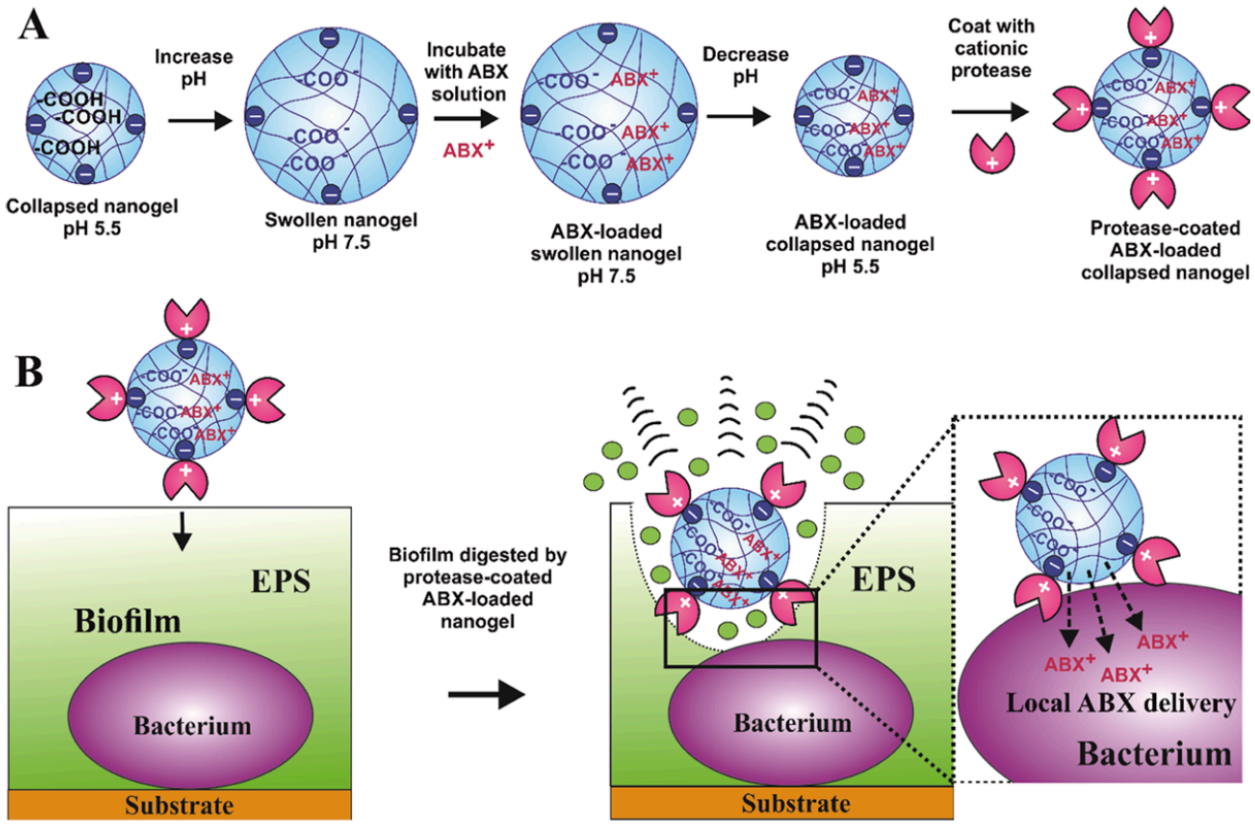

Scheme 1. (A) Antibiotic loaded Carbopol nanogel with a protease surface coating. (B) Carbopol/Alcalase nanogel particles on adherent biofilms.

The authors tested 3 types of formulations which are bare Carbopol nano gel, free Alcalase, and Carbopol/Alcalase nanogel. Bare carbopol nanogel was ineffective in biofilm biomass reduction. Compared to the carbopol nano gel, free Alcalase dramatically increased the ability to reduce biofilm bulk. The residual biofilm mass ranged from 80% to 40% with respect to the different bacteria species. Notably, the Alcalase-coated carbopol nanogel showed greater biofilm eradication than the free Alcalase. However, natural enzymes have drawbacks, including instability, quick deactivation, and high purification costs. Therefore, simulated enzymes [48] have been established it received a lot of attention recently in an effort to solve these problems. These enzymes are extremely stable, their catalytic activity is easily controllable, and they can be produced in vast quantities. Simulated enzymes also address the issue of essential enzymes limited permeability and shelf stability when used in biofilms [48].

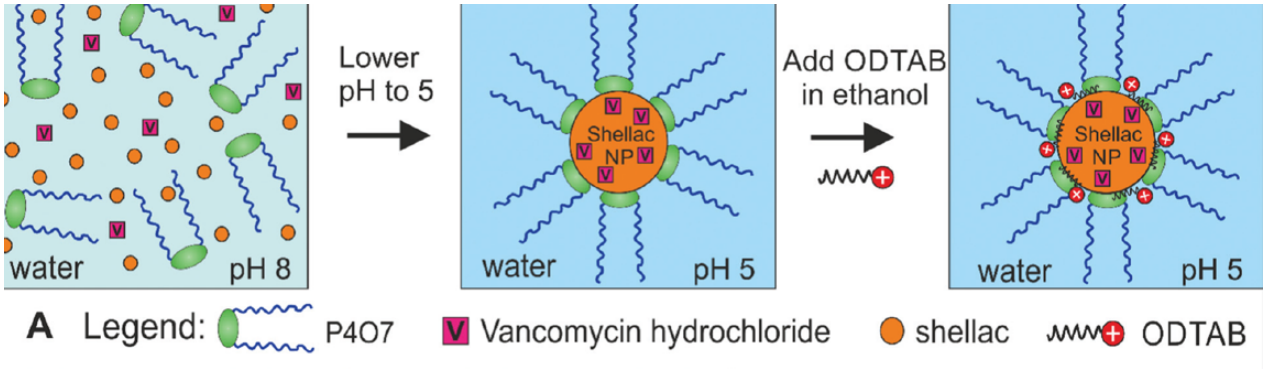

Scheme 2. Schematics of the two-step process for preparing dual functionalized Shellac nanocarriers for vancomycin antibiotic.

In a different study [49], shellac nanocarriers containing encapsulated antibiotic (vancomycin) encapsulation were produced, and their surfaces were functionalized, as is shown in Scheme 2. The antibiotic is retained in the shellac core because of hydrophobic and electrostatic interactions. The loaded vancomycin was released only close to the microbial cell wall as a result of electrostatic attraction between negatively charged shellac NPs and the negatively charged microbial cell membranes. A positive surface charge is provided by using the octadecyl trimethyl ammonium bromide (ODTAB) coating. It enhances its antibiotic impact on numerous microbial cells by enabling it to electrostatically adhere to the microbial cell walls and locally provide a high concentration of antibiotics. ODTAB was further used as a secondary surface treatment, allowing direct deposition on the shellac NPs surface. Despite the secondary coating with ODTAB reversing the surface charge, the nanocarrier kept its steric colloidal stability.

The antibiotic could be used in wound dressings for a long time since, once encased inside the shellac NPs, it can be released gradually. It should be noted that the shellac nanocarrier was produced using a "one-pot" method, making it simple to encapsulate and amplify the action of cationic antibiotics like vancomycin in the nanocarrier. Because ODTAB and Poloxamer 407 are present on the surface of the nanocarrier, this may increase permeability by electrostatically adhering a high local concentration of antibiotic/antimicrobial directly to

the microbial cell membrane. The authors show [49] that despite free vancomycin at the working concentration having a negligible antibacterial effect on yeast, algae, and Gram-negative bacteria like *E. coli*, its antimicrobial activity was diminished when combined with non-coated shellac nanocarriers. Hence the ODTAB coating is very essential for the nanoparticle antimicrobial activity.

As an alternative, another team [50] developed a cationic peptide-fullerene molecule that outperformed untreated fullerene in antibacterial photodynamic therapy (PDT), as it is illustrated in Scheme 3.

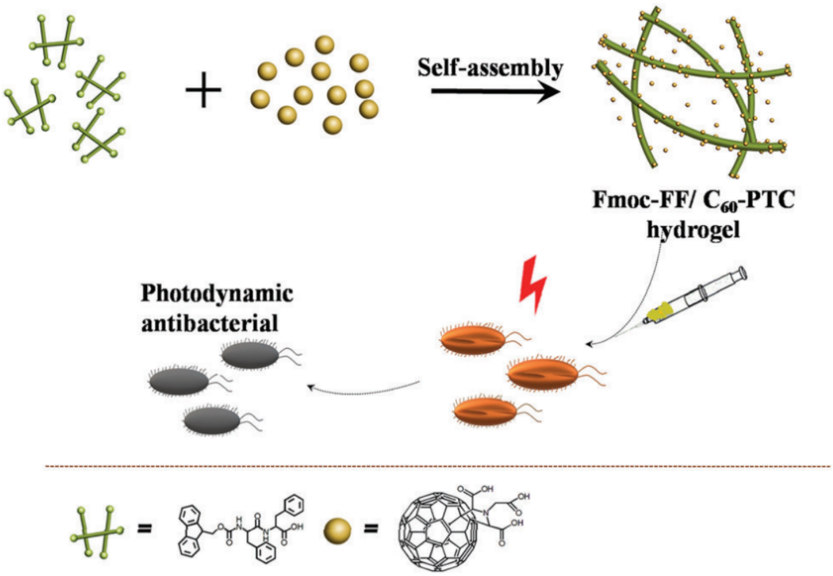

Scheme 3. Self-assembled peptide-fullerene hybrid hydrogels for PDT.

PDT, which uses reactive oxygen species (ROS) created by photosensitizers (PSs) and oxygen under light exposure to eliminate bacteria, is now recognized as a different efficient strategy with the benefit of having a minimal proclivity for drug resistance [51]. The mechanical properties of the peptide hydrogel are improved with fullerene, which makes the peptide hydrogel more durable and enhances targeted administration. This formulation has a positive impact on the degradation of *S. aureus* biofilm.

Another conducted research highlights the impact of berberine encapsulated in shellac nanoparticles on various bacterial strains [52]. This study demonstrates that these

microorganisms were sensitive to free berberine, which was not encapsulated in the nanoparticle. Due to electrostatic attraction between the negatively charged shellac NPs and the negatively charged bacterial cell membranes, which allows the encapsulated berberine to be released primarily onto the cell wall it amplifies the antimicrobial action of the nanoformulated berberine in cationically functionalized nanocarriers. In contrast, the antibacterial property of the non-coated shellac nanocarriers with encapsulated berberine was diminished compared with free berberine chloride.

A similar study [53] also examined the impact of shellac nanoparticles that were loaded with chlorhexidine, as in Scheme 4.

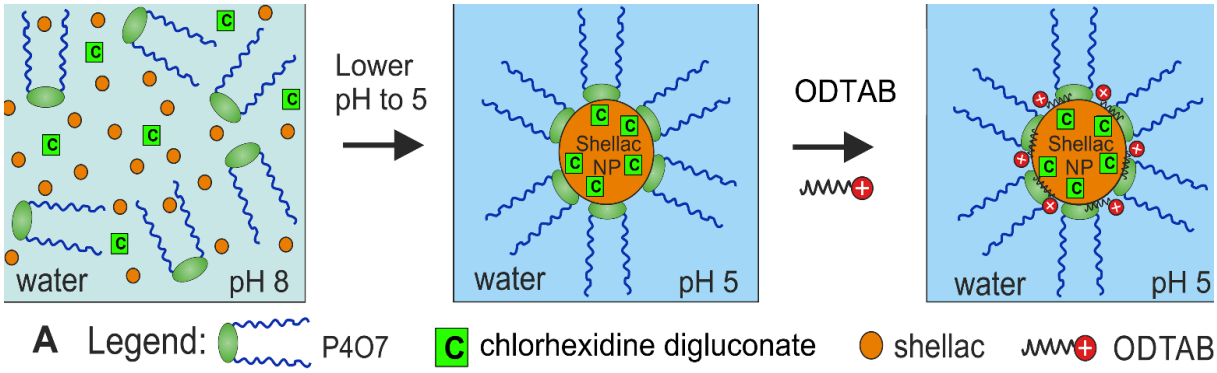

Scheme 4. Process flow diagram of sterically stabilized shellac nanoparticles with cationic surface functionality for chlorhexidine digluconate administration.

This methodology resembles the study with berberine, nevertheless the specified antibiotics varied from former research. The chlorhexidine was used as perfect candidate both in Gram-negative and Gram-positive bacteria. The effectiveness and side effects of the nano-formulations are mostly determined by the properties of the core materials used to create and functionalize the nanocarriers. Shellac was a primary ingredient in their research. It was employed as a result of its widespread use in tablet enteric coatings and as a pharmaceutical encapsulating agent. It is the sole therapeutic resin made from an insect and approved by FDA. Bleached shellac is a complex mixture of polar and non-polar polyhydroxy shelloic acids, it is essentially insoluble in water at neutral and acidic pH. Due to its biocompatibility, shellac is a

viable core material for the creation of drug nanoparticles [54]. The outcomes of the research revealed that uncoated shellac NPs even when loaded with chlorhexidine did not show a great impact on microorganisms. The shelloic acid, carboxylic groups, and chlorhexidine interact, and free chlorhexidine drastically suppresses slows down its release and hence its impact on yeast and *E. coli* bacteria. Hence, when chlorhexidine was entrapped in shellac particles, it was less effective, proving the conclusion of better efficiency as a free agent in solution at the same concentration. When an ODTAB coating was added in the second stage it led to higher adhesive properties of NPs to the target cells. The antibacterial property of chlorhexidine was significantly boosted when loaded within shellac NPs further coated with ODTAB in comparison with other nanocarriers or as a free agent in solution. Additionally, ODTAB enhances the ability of chlorhexidine to eradicate bacteria with small proportions. As scholars state, it is possible to apply this combination for the development of treatment for wounds and the synthesis of antibiotics.

Strategy pursued in the present study

Considering the recent highlights and progress in the impact of NPs on the treatment of bacterial infections, the current study suggests the non-invasive approach utilizing medical ultrasound as a possible solution to this problem of stimulus triggered degradation of bacterial biofilms. Utilizing US simultaneously with NPs deposited on surfaces prone to develop bacterial biofilm infection would benefit the disruption of the bacterial biofilm EPS and, therefore, accelerate the healing of chronic wounds. As is noticed in the recent contributions, the physical method, which is scraping, carries negative consequences such as excess bleeding, pain, infection, loss of healthy tissue, and delayed healing. To avoid these side effects, nanoparticles based on shellac and enzyme coated with silica shell can be used simultaneously with ultrasound which leads to fracturing of the shell and allow the enzyme to spread within the EPS in therapeutic quantities.

Shellac was chosen as a nanocarrier material because of its biodegradability and biocompatibility. Polar and non-polar substances such as lactones, anhydrides, and polyhydroxy acids are combined in shellac. Additionally, the neutral and acidic conditions that are used in the present methods to dissolve shellac are intractable. With a few minor alterations, the current technique for the project detailed in this report is similar to that of the articles mentioned above. The modifications include the encapsulation of enzymes like Alcalase, Savinase, and cellulase rather than antibiotics and antimicrobials. The same stabilizing ingredient is Poloxamer 407, a non-ionic copolymer made of poly(ethylene oxide), poly(propylene oxide), and poly(butadiene oxide) (ethylene oxide). It is frequently utilized as an emulsifying, dispersing, stabilizing, and surfactant agent [11]. Also, the above-mentioned studies utilized ODTAB, a water insoluble cationic surfactant, as a secondary functionalization agent to convert the negative surface charge of the nanoparticles to a positive surface charge. However, the shellac core will be coated with the silica by using two different precursors (TEOS or APTES) that is already positively charged in the present approach. The creation of silica-coated shellac/enzyme nanoparticles and their ultrasound-based triggering mechanism for release of the enzyme in the biofilm is shown in Scheme 5.

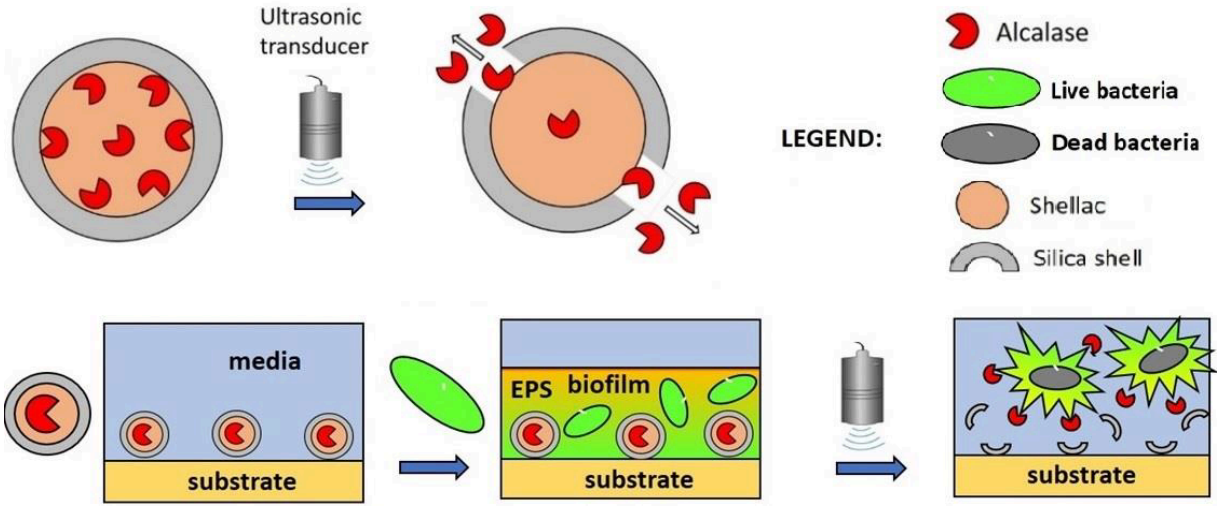

Scheme 5. The mechanism of triggered release of silica-coated enzyme-loaded shellac nanoparticles and their rupture by using ultrasound (US). The particles are used to pre-

coat surfaces prone to developing bacterial biofilms to facilitate their US triggered enzyme release and biofilm degradation.

The current study focuses on the formation of core-shell NPs, which are loaded with an enzyme of choice as an active component that can disrupt and degrade bacterial biofilms. Therefore, the first stage of the project was to develop the shellac/poloxamer 407 NPs without the enzyme payload to verify their compatibility and parameters such as size and zeta potential. The enzyme was encapsulated via co-precipitation with shellac in the presence of surface-active polymer. The preparation of the enzyme-loaded shellac particles is very similar to the process of illustrated in Scheme 4 where the enzyme is co-precipitated instead of antimicrobial (chlorhexidine). Once the enzyme is encapsulated within the particle core, a silica coat needs to be developed to protect the enzyme from premature release. After the enzyme-loaded shellac nanoparticles (coated with silica shell or non-coated) were produced and characterized, a bacterial study was performed that includes the growing bacterial biofilms on the substrates will demonstrate how the NPs can digest and degrade the biofilm EPS upon US trigger.

The potential advantages of our approach are that as biofilm grows on the pretreated surfaces, the enzyme is released from the NPs only within the EPS, which would reduce side effects. The proposed treatment is the non-invasive that does not involve the side effects as in the case of scraping, biocompatibility, and biodegradability of the NPs components. Also, the NPs which have the silica coating are more stable and would have longer shelf life than uncoated enzyme loaded NPs. This allows for triggered release of the enzyme and potentially higher enzyme concentration thus leading to higher biofilm degradation.

3 Results and Discussion

3.1. Synthesis of unloaded and uncoated Shellac/Poloxamer 407 nanoparticles

We use shellac as a core of the nanoparticle matrix, poloxamer 407, to stabilize and protect the shellac nanoparticles from precipitation at the acidic condition at which NPs synthesis is done. This colloidal stabilization is based on the steric repulsion mechanism by surface layers of poloxamer 407. Bare shellac is not stable in acidic conditions and precipitates immediately in an uncontrolled way. To be precise, carboxylic acid -COOH and hydroxyl -OH groups undergo protonation, which results in electroneutral -COOH groups. This reduces the solubility of shellac in water and leads to its insolubility and precipitation that creates colloid particles. Therefore, poloxamer 407 is used to stabilize them. P407 has amphiphilic nature and consists of hydrophobic poly(propylene oxide) (PPO) blocks that adsorb on hydrophobic shellac, while hydrophilic poly(ethylene oxide) (PEO) surrounds the surface of the nanoparticle. The reason for the stabilization of shellac NPs is steric repulsion between polyethoxy chains on the surfaces of approaching particles in aqueous media.

Figure 4 shows the results of dynamic light scattering measurements using Litesizer500 (Anton Paar, Austria). It demonstrates the average particle size and zeta potential of unloaded and uncoated Shellac/Poloxamer 407 nanoparticles. At pH 4, the average hydrodynamic diameter is 81±1 nm, and the zeta potential is –3±1 mV. As was observed previously [52], average particle size does not depend on the pH as once formed they are stabilized by steric stabilization. Once the nanoparticles are produced, the average particle sizes have similar values and almost do not change. However, zeta potential is sensitive to changes in acidity. Also, due to the presence of a -COOH group on the surface that undergoes deprotonation and becomes negatively charged in $-COO^-$ form, the zeta potential of NPs tends to have a more negative charge overall, decreasing up to -18±1 mV at pH 8.

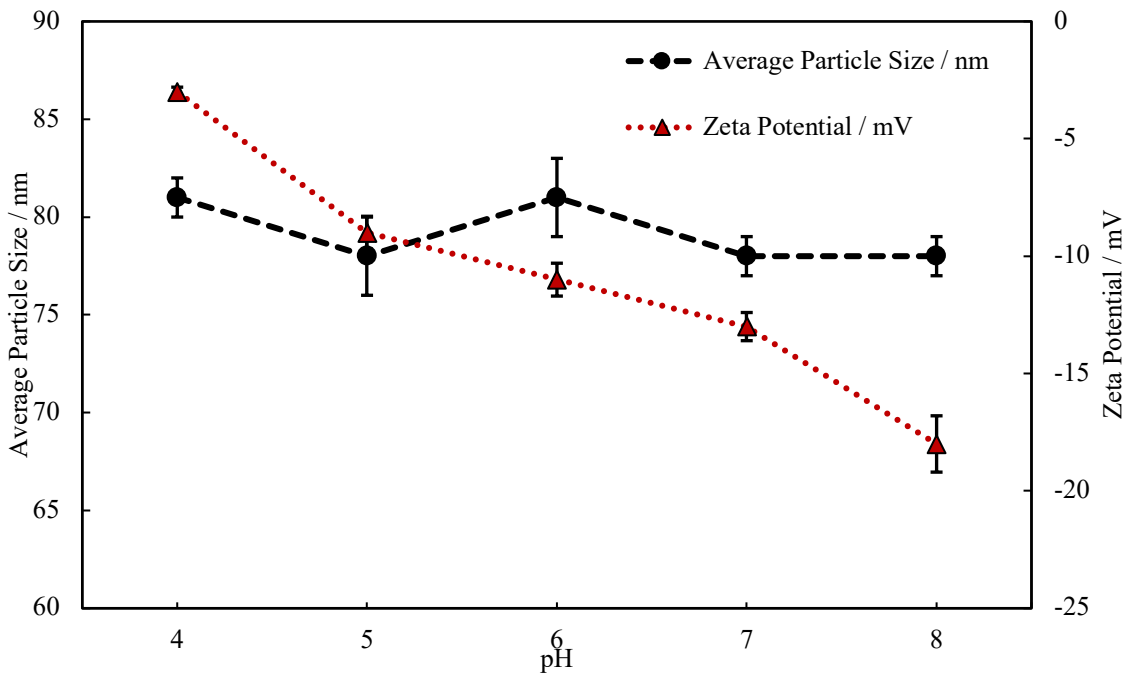

Figure 4. Average particle size and zeta potential of 0.125wt% Shellac/0.125 wt% Poloxamer 407 NPs.

3.2. Encapsulation of enzymes to the shellac core

To investigate the effectiveness of encapsulation of a number of enzymes (Alcalase, Savinase, Cellulase) when loaded into the shellac core, the experiment was done with different enzyme concentrations at pH 4. Low enzyme concentrations, which is 0.05wt%, did not show changes in the average particle size nor in their average zeta potential values. However, if enzyme concentrations are increased from 0.1wt% to 0.15wt%, the average particle size starts to increase. The zeta potential does not change significantly. At concentrations of enzyme 0.3wt% and 0.35wt%, the size is decreased because it is possible that the shellac cannot incorporate larger concentrations of enzyme (i.e., the enzyme content becomes bigger than the shellac matrix of the particle, which changes the dynamics of the co-precipitation process).

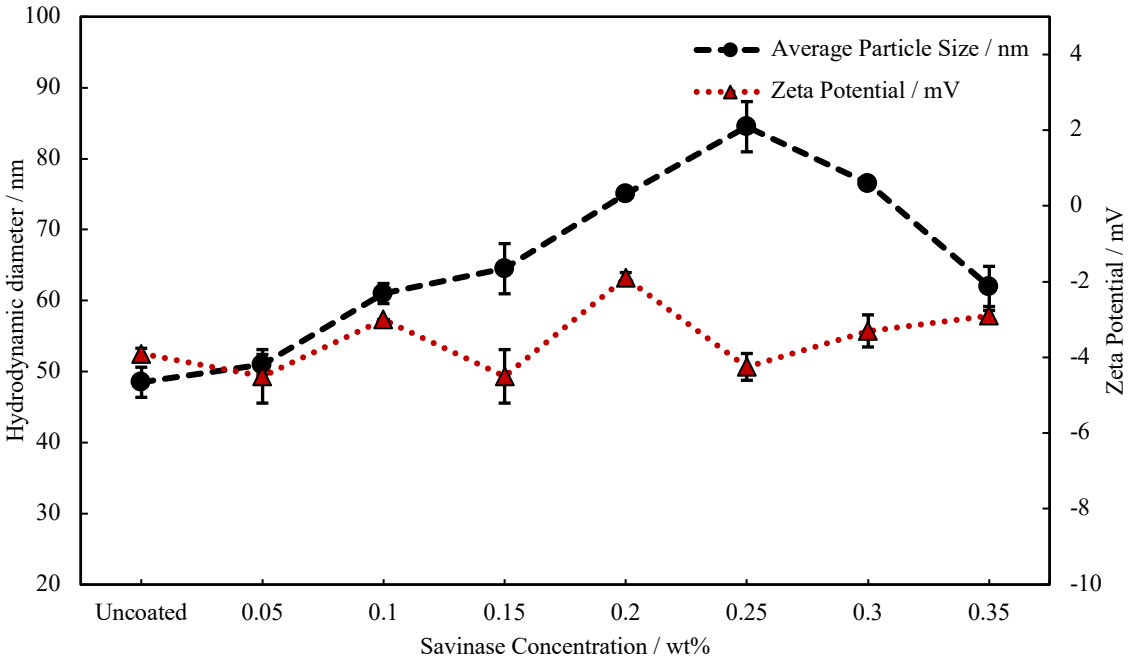

Figure 5. Average particle size and zeta potential of enzyme-loaded Shellac NPs stabilized by Poloxamer 407 vs the Savinase concentration.

Figure 6 shows the TEM images of uncoated Alcalase-loaded shellac NPs. Direct measurements of the particle size from the TEM images yields an average size of 56±7 nm, which is different from that of the DLS measurements, which illustrates that the size of shellac NPs loaded with 0.15wt% Alcalase is 64±4 nm. The observed discrepancies in the size are because DLS measures it in the liquid state that contributes to the bigger size (expanded poly ethoxy chains), while in TEM, the samples are dried and the liquid layer is removed.

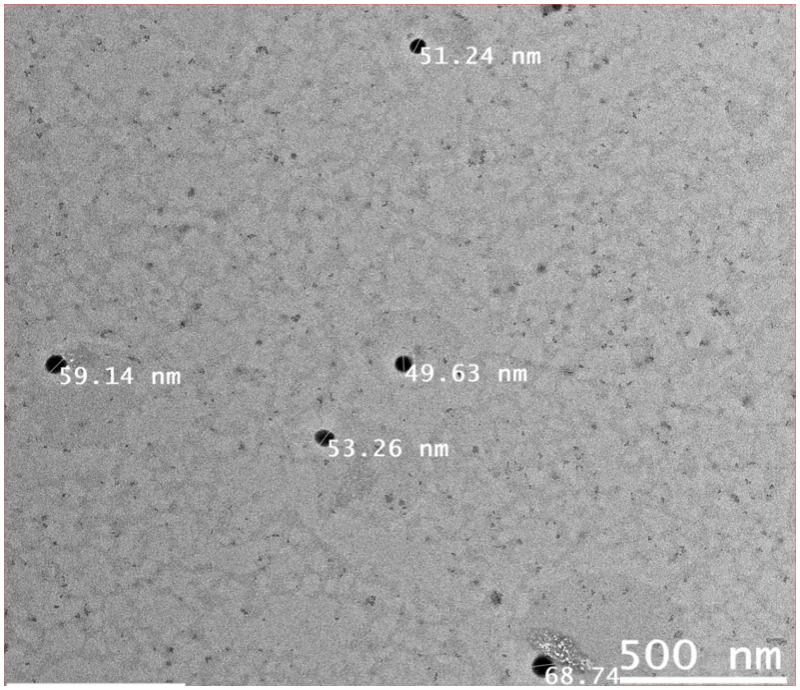

Figure 6. TEM images of uncoated 0.125wt% Shellac/0.15wt% Alcalase NPs.

SEM images in Figure 7 demonstrate the average size of 62±8 nm. Observed NPs are small in size, so SEM cannot clearly show them in a good resolution as samples overheats upon focusing which is causing local expansion. In addition, residual solutes from the suspension deposit upon evaporation which slightly amends the particles size. Note that the sample is coated with 10 nm gold layer as a part of the sample preparation for SEM imaging.

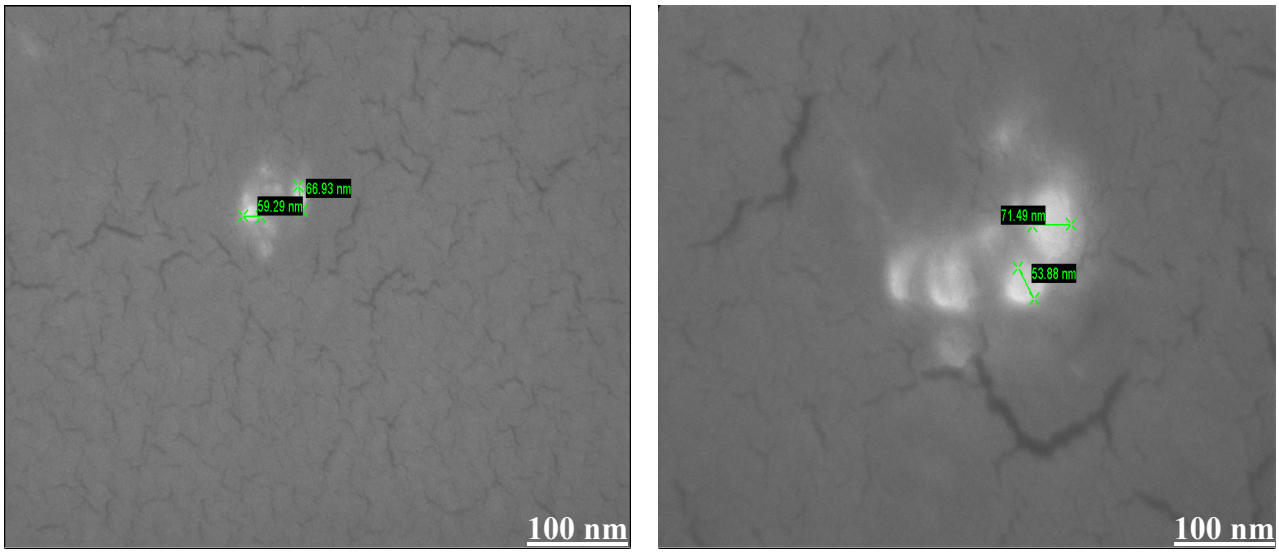

Figure 7. SEM images of uncoated 0.125wt% Shellac NPs loaded with 0.15wt% Alcalase.

3.3. Coating of shellac NPs with silica precursor – APTES

In the first stage of the study we attempted to coat the shellac/enzyme NPs with (3-Aminopropyl)triethoxysilane. APTES is an organosilane compound comprising a triethoxysilane group ($Si(OC_2H_5)_3$) and an aminopropyl group ($-NH(CH_2)_3-$). It is subjected to hydrolysis and polycondensation reactions. Also, the ethoxy groups (OC_2H_5) of APTES react with water and result in the release of ethanol (C_2H_5OH) and the creation of silanol groups (Si-OH). Further polycondensation processes can subsequently occur, culminating in the production of a matrix of siloxane linkages (Si-O-Si) conjugated with 3-aminopropyl groups. In this study, we implemented the coating process under ambient and high temperatures.

As shown in Figure 8, upon acidic hydrolysis at pH 3, the particle size grows until a certain point after 4 hours, then slightly decreases. The possible explanation for it is that under ambient temperature, the coating reaches its limit approximately after 2 hours of hydrolysis of APTES precursor. Note that the surface charge changes as more amino groups are added to the shell from the APTES residues. Moreover, silica is very sensitive to temperature. Therefore, it is necessary to test the APTES under high-temperature conditions to compare the results.

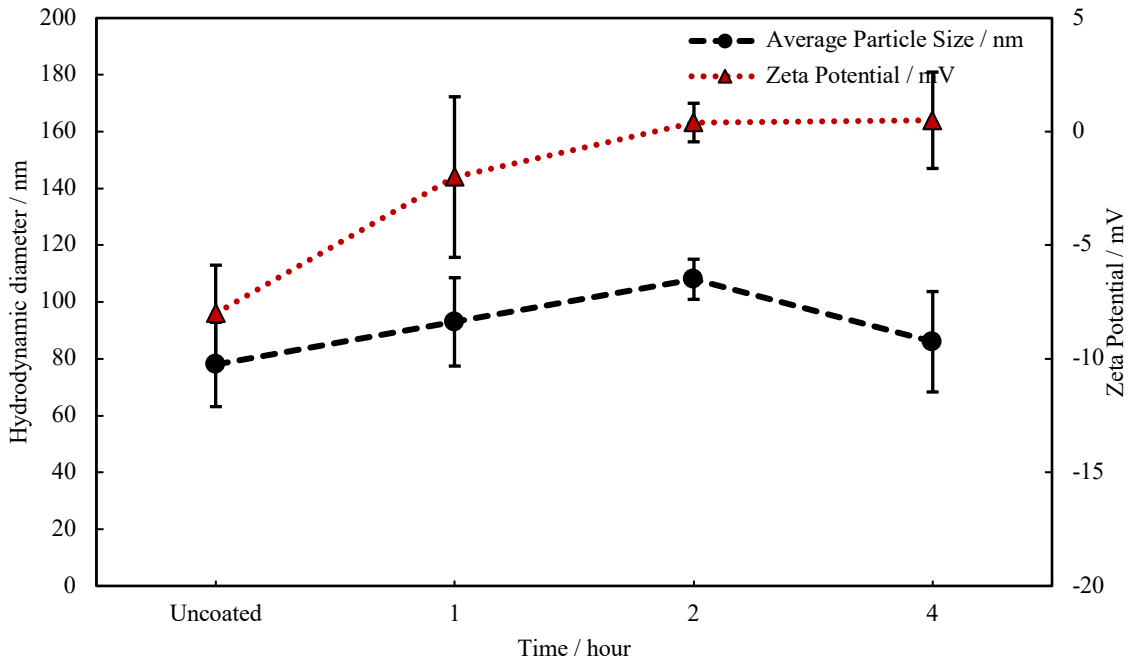

Figure 8. 0.06 wt% APTES coating of 0.06wt%/0.05wt% Shellac/Poloxamer 407 NPs average particle size and zeta potential.

Compared to coating shellac NPs with APTES at ambient conditions, the higher temperature of hydrolysis positively affects the particle size growth and zeta potential. Figure 9 demonstrates a drastic increase in the size from 48 nm to 92 nm within 1 hour of coating. It implies that APTES starts to hydrolyze faster under heating of the system at 55°C and reaches colloidal stability faster than the coating under ambient temperature. The zeta potential increases from -10 mV to -2 mV, and it clearly shows that APTES covered the shellac NPs surface. Both particle size and zeta-potential level off after 3 hours of coating.

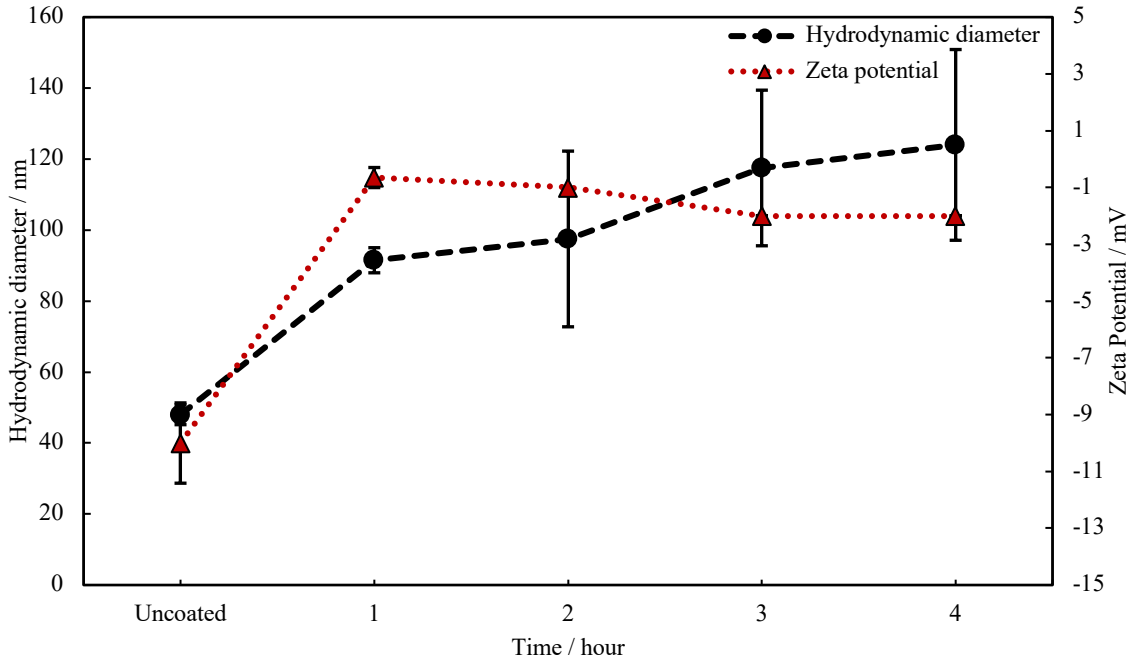

Figure 9. Average particle size and zeta potential of organosilica-coated 0.06wt%/0.05wt% Shellac/Poloxamer 407 NPs obtained by hydrolysis of 0.05 wt% APTES at pH 3 at 55°C.

Figure 10 shows the TEM images of APTES-coated shellac NPs at 55°C under acidic conditions. The NPs have a spherical shape and smooth surface without grains. The sizes range from 50 nm to 87 nm. Also, there is an indication of a shell because the inorganic materials, such as silica, become lighter in color than the core, which is the specificity of TEM.

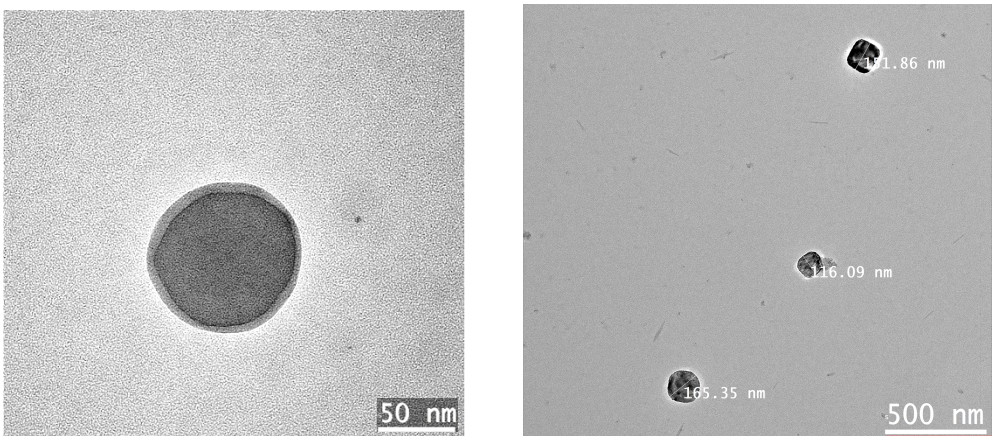

Figure 10. Typical TEM images of organosilica coated shellac NPs obtained by APTES hydrolysis at pH 3 at temperature 55℃.

3.4. Coating of shellac NPs with silica precursor - TEOS

In addition to the APTES coating, we performed coating of the shellac NPs using tetraethyl orthosilicate (TEOS) silica precursor. It is a popular precursor in the production of silica-based compounds. Similar to APTES, it is an organosilicon compound consisting of $Si(OC_2H_5)_4$. To produce silica matrix, TEOS undergoes hydrolysis and condensation processes. When TEOS is subjected to aqueous hydrolysis, it undergoes similar processes as APTES. These polycondensation events result in the creation of siloxane linkages (Si-O-Si), which results in the construction of a three-dimensional silica network. The hydrolysis of TEOS can be done both at high and low pH where the catalysts are OH^- and H^+, respectively.

In Figure 11, the DLS data show that the average size of the particles gradually increases within 4 hours period. It starts from 68±2 nm for uncoated NPs and goes up to 200±55 nm. Also, the zeta potential does not significantly change its values. The changes in the zeta potential from -3 mV of uncoated shellac nanoparticles to the endpoint of 4 hours of synthesis, which is -7 mV, indicate that the negatively charged TEOS has covered the surface of the shellac core.

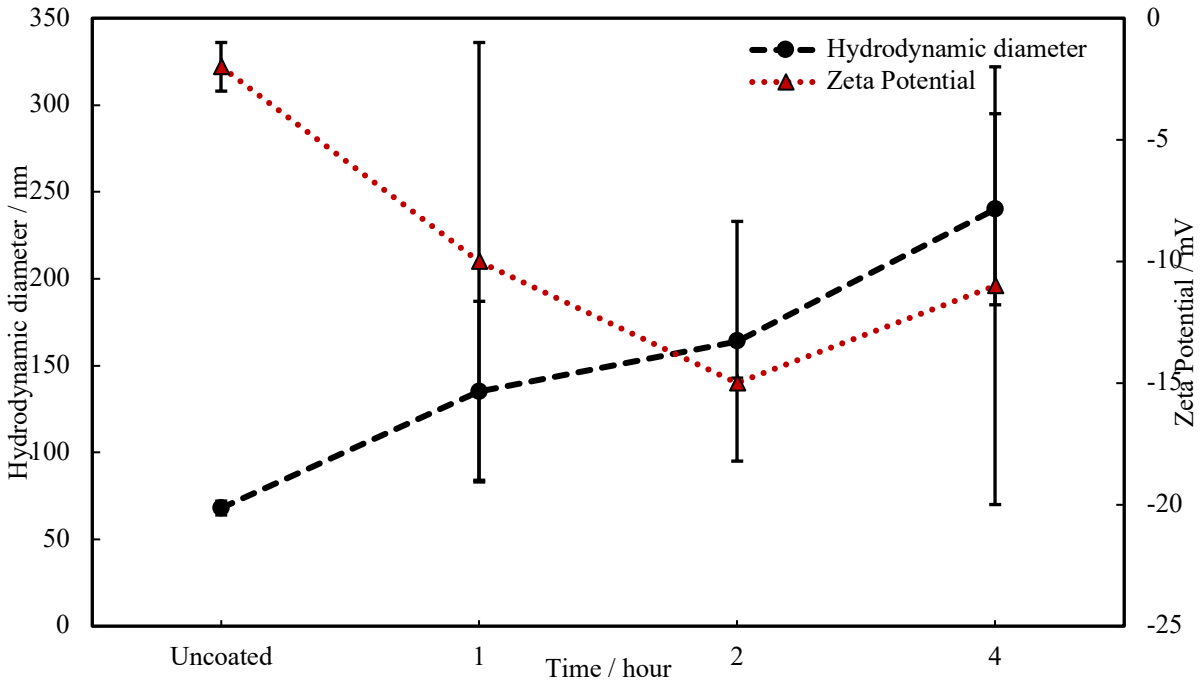

Figure 11. Average particle size and zeta potential of TEOS coated shellac NPs.

Figure 12 shows the TEM images of the TEOS-coated shellac NPs. There is a visible border between TEOS and the shellac core. Particularly, TEOS has a lighter tone (as it is peripheral layer), and shellac is darker as it is the core. Also, the average particle sizes that can be shown from TEM image measurements are slightly different from the DLS measurements due to the fact that DLS measures the size in solution. However, on TEM, the nanoparticles can be captured individually, and therefore different sizes of nanoparticles can be observed and investigated. Nevertheless, the average particle size form DLS and TEM are in a similar range.

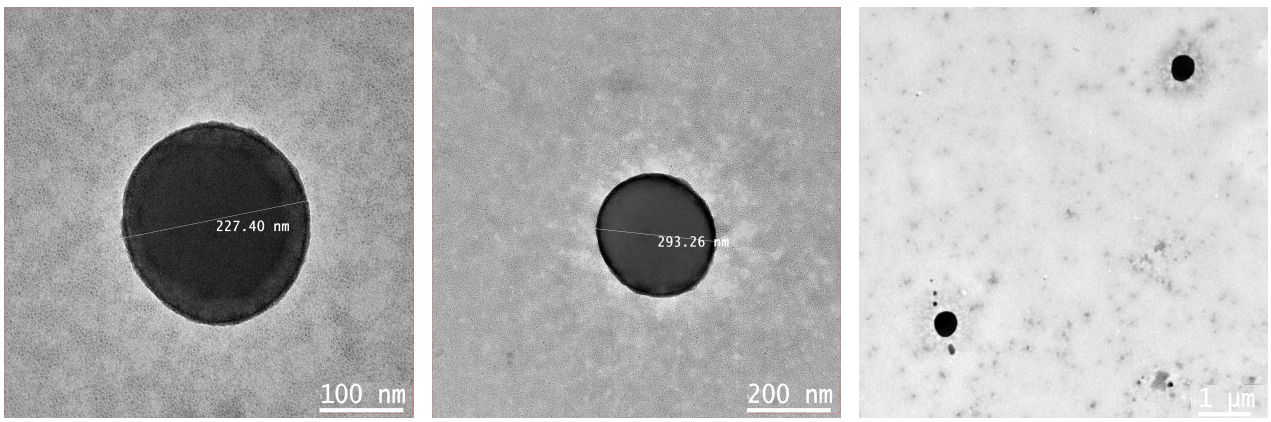

Figure 12. Typical TEM images of silica coated shellac NPs 0.06wt%/0.05wt% obtained by 0.1 wt% TEOS hydrolyzed at pH 4.

According to SEM images on Figure 13, the sizes of TEOS-coated shellac/enzyme NPs vary between 98 nm to 145 nm. Comparing DLS measurements, TEM images with SEM, the sizes of NPs are different. DLS measures the hydrodynamic size of NPs with the surrounding solvent that forms the hydration layer. Therefore, the estimated hydrodynamic size is larger than the dry size of NPs. However, the samples for TEM and SEM are visualized under a vacuum and require dried samples. We suggest that SEM imaging gives lower resolution and magnification. Therefore, our NPs are poorly visible by SEM, it is impossible to see the detailed structure of the coating shell. In addition, when zooming into the sample, the focus is lost due to local overheating, and the image becomes fuzzy.

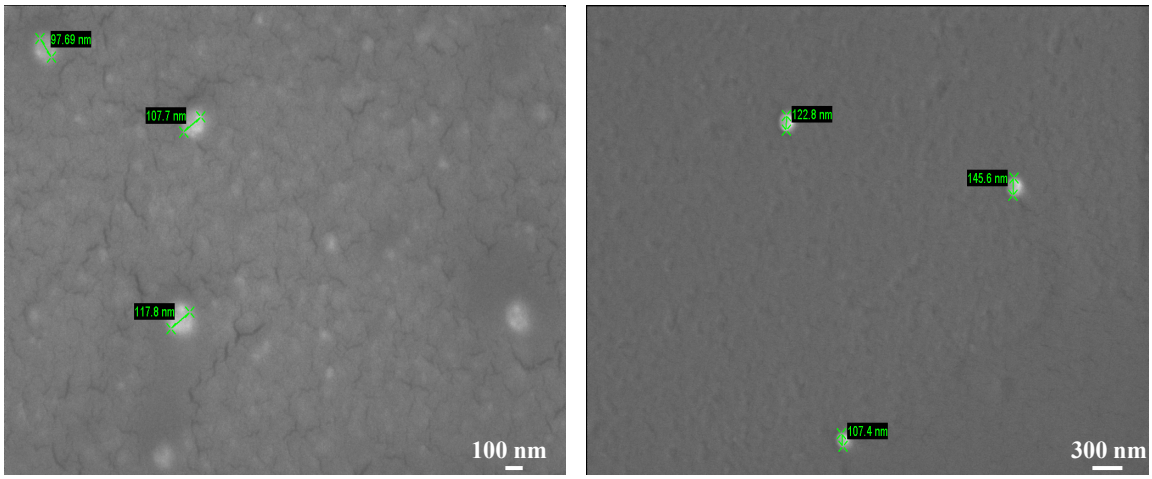

Figure 13. Typical SEM images of TEOS-coated Shellac/Enzyme NPs.

3.5. EDS analysis of uncoated and TEOS-coated Shellac/Enzyme NPs

In order to investigate the presence of nitrogen, which is an indication of enzymes in the NPs, we conducted Energy Dispersive X-Ray Spectroscopy. Enzymes contain amino groups -N–H, which serve as the building blocks. Amino groups participate in hydrogen bonding and operate as proton acceptors or donors. Figures 14 (A) and (B) show the presence

of nitrogen as an indication of encapsulated alcalase and savinase. In shellac/alcalase NPs mass% of nitrogen is 6±0.17, while in shellac/savinase NPs it is 6±0.1 mass%.

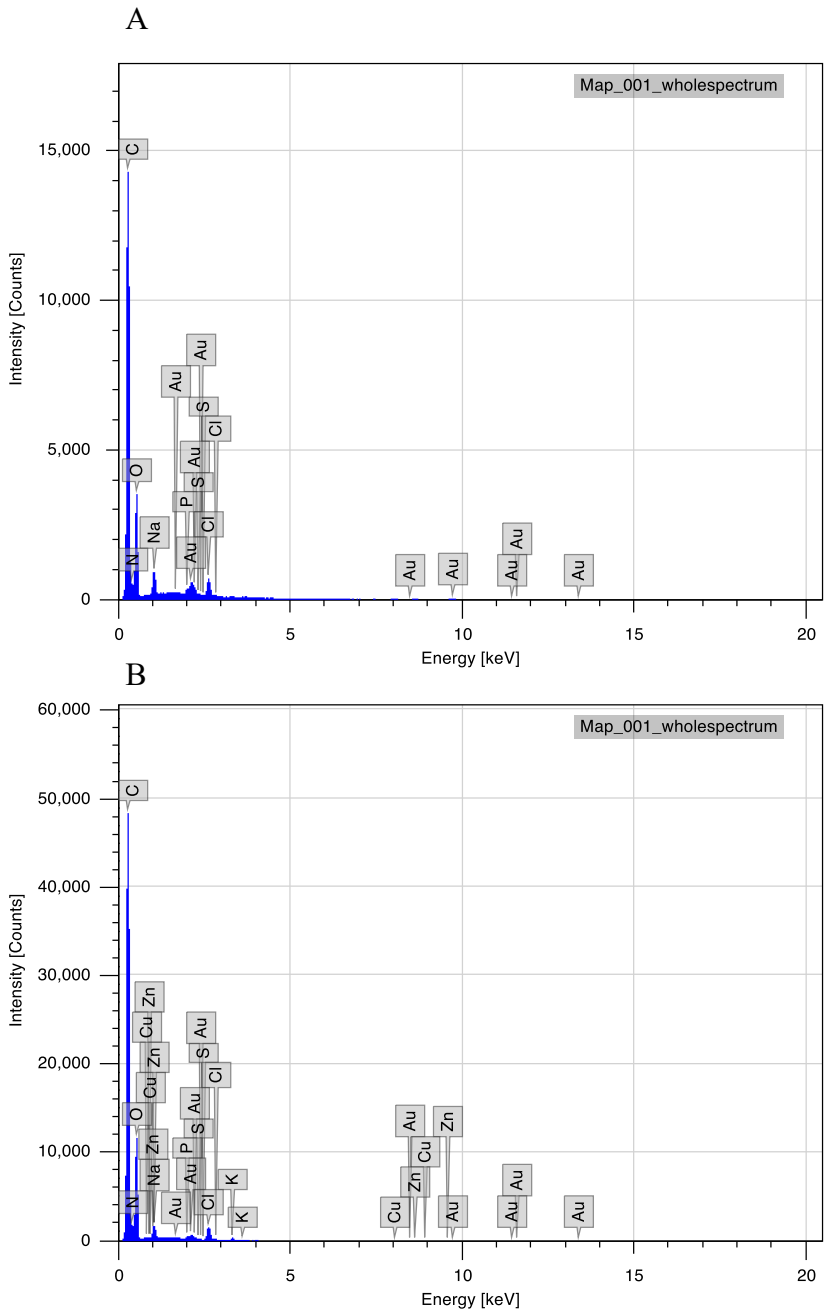

Figure 14. (A) EDS spectra elemental analysis of uncoated shellac/alcalase NPs, (B) EDS spectra elemental analysis of uncoated shellac/savinase NPs.

Another element that is present in the coated shellac NPs is silica Si. It comes from the TEOS coating. According to Figure 15, the EDS shows 46±0.08 mass% of carbon, 36±0.11

mass% of oxygen, and 6±0.04 mass% of silica. Due to the presence of TEOS coating on the surface of NPs, silica is detected in EDS.

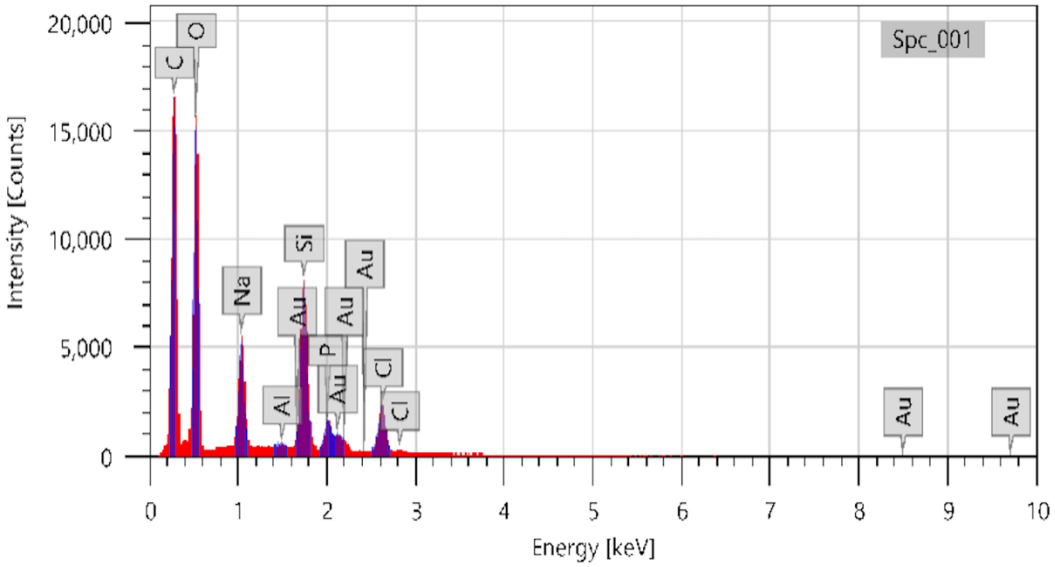

Figure 15. EDS spectra elemental analysis of silica-coated shellac NPs.

3.6. Fourier Transform Infrared spectroscopy (FTIR)

To characterize the prepared shellac NPs, FTIR spectroscopy (performed using Thermo Scientific Nicolet iS10 FT-IR Spectrometer, USA) is used. Figure 16 shows the FT-IR spectra for the uncoated and coated Alcalase-loaded NPs.

The shellac spectrum (blue line) presents a main broad peak at 3358 cm^{-1} that is an indication of the O–H stretching vibration band. Also, the 1708 cm^{-1} peak belongs to the carbonyl stretching vibration band C=O, and a peak at 1252 cm^{-1} is a C–O stretching band. Spectrum for the P407 (brown line) demonstrates C–H aliphatic stretching at 2877 cm^{-1}, at 1341 cm^{-1} there is an in-plane O–H bend. Moreover, peak at 1096 cm^{-1} belongs to the C–O stretch.

The alcalase spectrum (green line) shows characteristic peaks at 3262 cm^{-1}, indicating the O–H stretching vibration band. The peak at 1646 cm^{-1} is carbonyl stretching vibration band C=O that is associated with amide I, peak at 1470 cm^{-1} is for amide II N–H bending and C–N stretching. Also, the peak at 1038 cm^{-1} corresponds to C–O stretching band.

The TEOS spectrum (black line) shows peaks at 2974 cm^{-1} which relates to the C–H stretching vibration, 1073 cm^{-1} peak corresponds to the asymmetric stretching vibration of Si–O–Si bonds. Also, 958 cm^{-1} and 784 cm^{-1} peaks relate to the symmetric and bending vibrations respectively for Si–O–Si bonds.

For the uncoated alcalase-loaded NPs (red line), peaks at 3262 cm^{-1} and 1636 cm^{-1} that come from shellac and alcalase overlap, indicating that alcalase is encapsulated inside the shellac core. Peaks from P407 are united with shellac because there is no chemical reaction between P407 and shellac. Particularly, there is an adsorption of hydrophobic PPO of P407 on the surface of shellac, so peaks at1392 cm^{-1} and 1066 cm^{-1} still exist, but they are not prominent.

For the TEOS-coated Alcalase-loaded shellac NPs (purple line), peak at 3354 cm^{-1} indicates O–H stretching vibration that overlaps with shellac and alcalase. Peaks at 2921 cm^{-1} and 2852 cm^{-1} are C–H stretching from shellac, alcalase, and P407. 1636 cm^{-1} peak comes from C=O stretching that overlap with shellac, alcalase and P407. Additionally, peaks at 1252 cm^{-1} represent C–O stretching and 1074 cm^{-1} is for Si–O bonds that come from TEOS. Therefore, FTIR spectra confirm the Alcalase encapsulation and TEOS coating of shellac NPs.

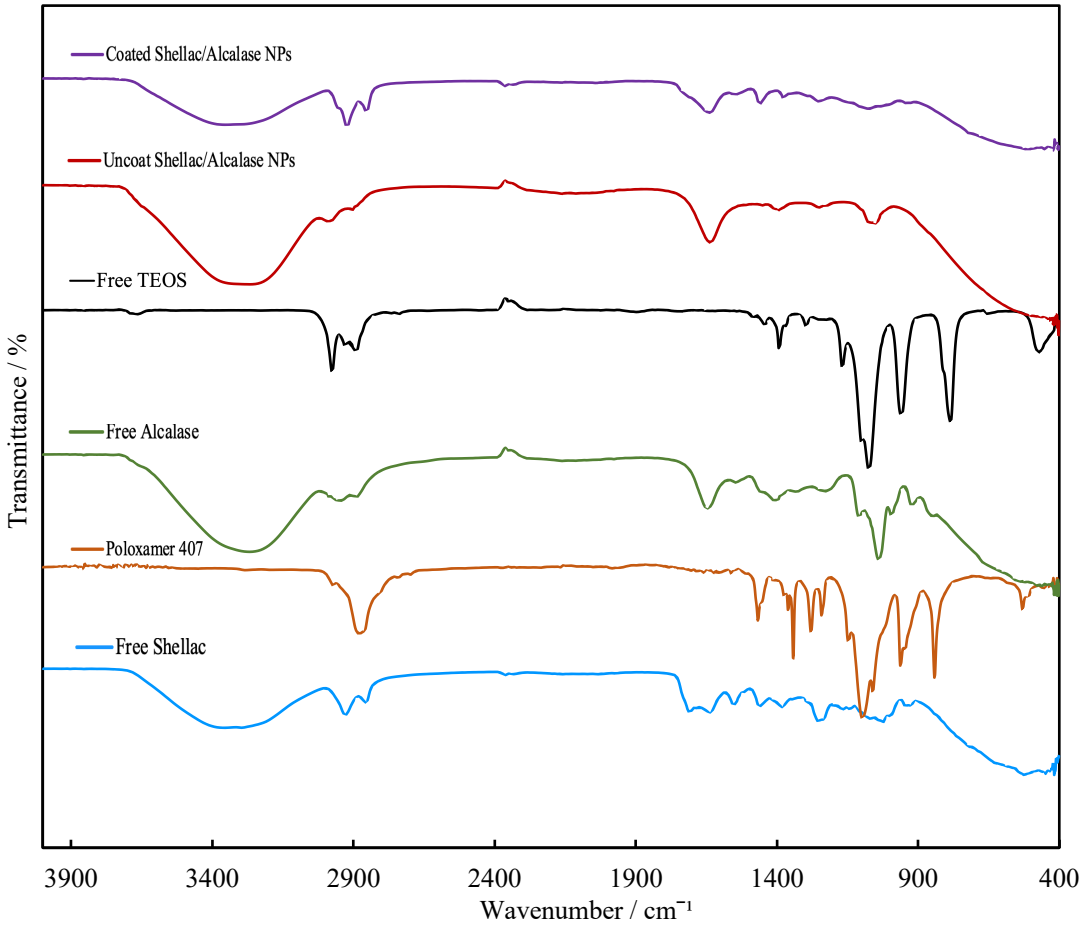

Figure 16. FT-IR spectra of free shellac, free P407, free alcalase, free TEOS, uncoated Alcalase-loaded shellac NPs, silica-coated Alcalase-loaded shellac NPs (from TEOS precursor).

Figure 17 shows the FTIR spectra for uncoated Savinase-loaded shellac NPs, and TEOS-coated Savinase-loaded shellac NPs. Savinase spectrum (green line) contains peak 3273 cm^{-1} that corresponds to the O–H stretching vibration, 1647 cm^{-1} peak indicates C=O stretching in amide groups of the peptide backbone, 1037 cm^{-1} is associated with C–O or C–N stretching. For the uncoated Savinase-loaded NPs (red line), peaks at 3339 cm^{-1} and 1636 cm^{-1} that come from shellac and Savinase overlap, indicating that Savinase is encapsulated inside the shellac core.

For the silica-coated Savinase-loaded shellac NPs (purple line), peak at 3261 cm^{-1} indicates O–H stretching vibration that overlaps with shellac and Savinase. 1636 cm^{-1} peak

comes from C=O stretching that overlap with shellac, Savinase and P407. Additionally, peak at 1393 cm^{-1} represent C–H bending and 1045 cm^{-1} is for Si–O bonds that come from TEOS. Therefore, FTIR spectra confirm the Savinase encapsulation and TEOS coating of shellac NPs.

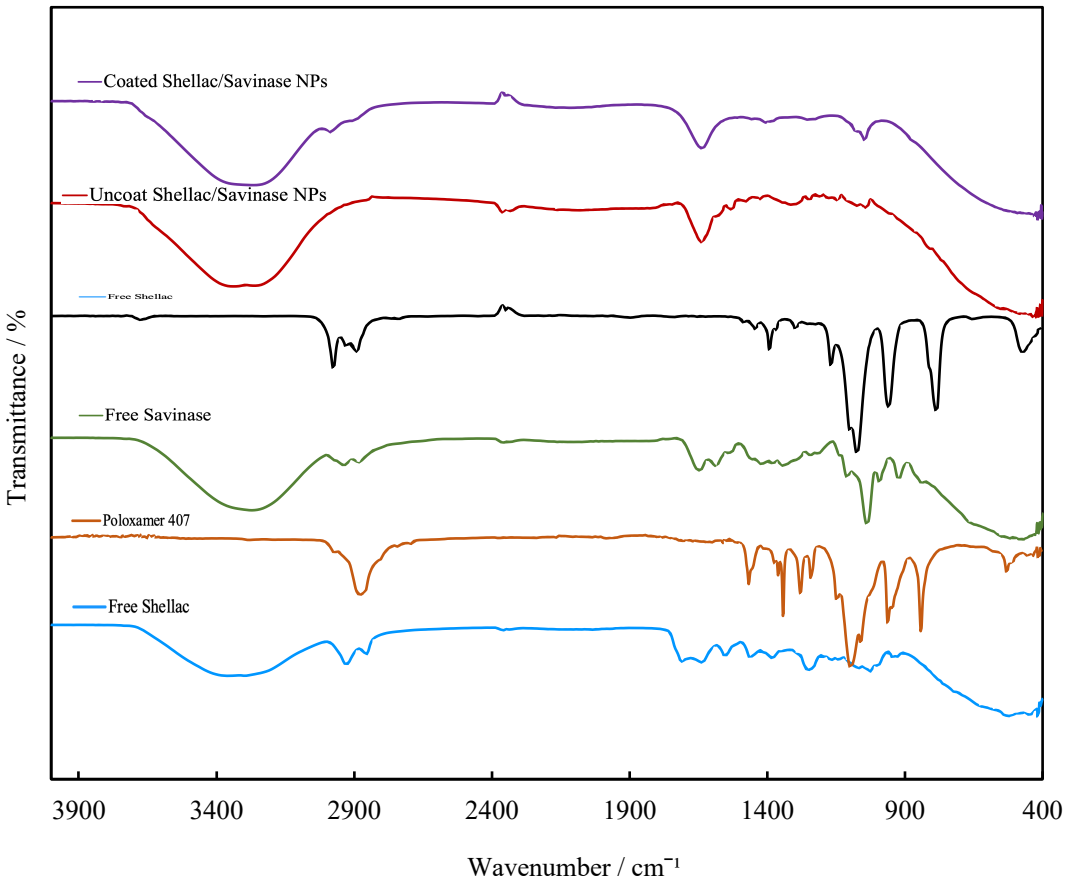

Figure 17. FT-IR spectra of free shellac, free P407, free savinase, free TEOS, uncoated Savinase-loaded shellac NPs, TEOS-coated Savinase-loaded shellac NPs.

Figure 18 demonstrates the FTIR spectra for the uncoated Cellulase-loaded shellac NPs, TEOS-coated Cellulase-loaded shellac NPs. Cellulase spectrum (green line) 3279 cm^{-1} belongs to the O–H stretching vibration. Peak at 1635 cm^{-1} is associated with amide I that corresponds to C=O stretching in the amide groups of the peptide backbone. Also, 992 cm^{-1} peak is attributed to the C–O or C–N stretching. For the uncoated cellulase-loaded NPs (red line), peaks at 3265 cm^{-1} and 1636 cm^{-1} that come from shellac and cellulase overlap, indicating that cellulase is encapsulated inside the shellac core.

For the silica-coated Alcalase-loaded shellac NPs (purple line), a peak at 3335 cm^{-1} indicates O–H stretching vibration that overlaps with shellac and cellulase. Peaks at 2921 cm^{-1} and 2852 cm^{-1} are C–H stretching from shellac, cellulase, and P407. 1639 cm^{-1} peak comes from C=O stretching that overlaps with shellac, cellulase and P407. Additionally, the peak at 1044 cm^{-1} is for Si–O bonds that come from TEOS but it is not prominent. Therefore, FT-IR spectra confirm the Cellulase encapsulation and TEOS coating of shellac NPs.

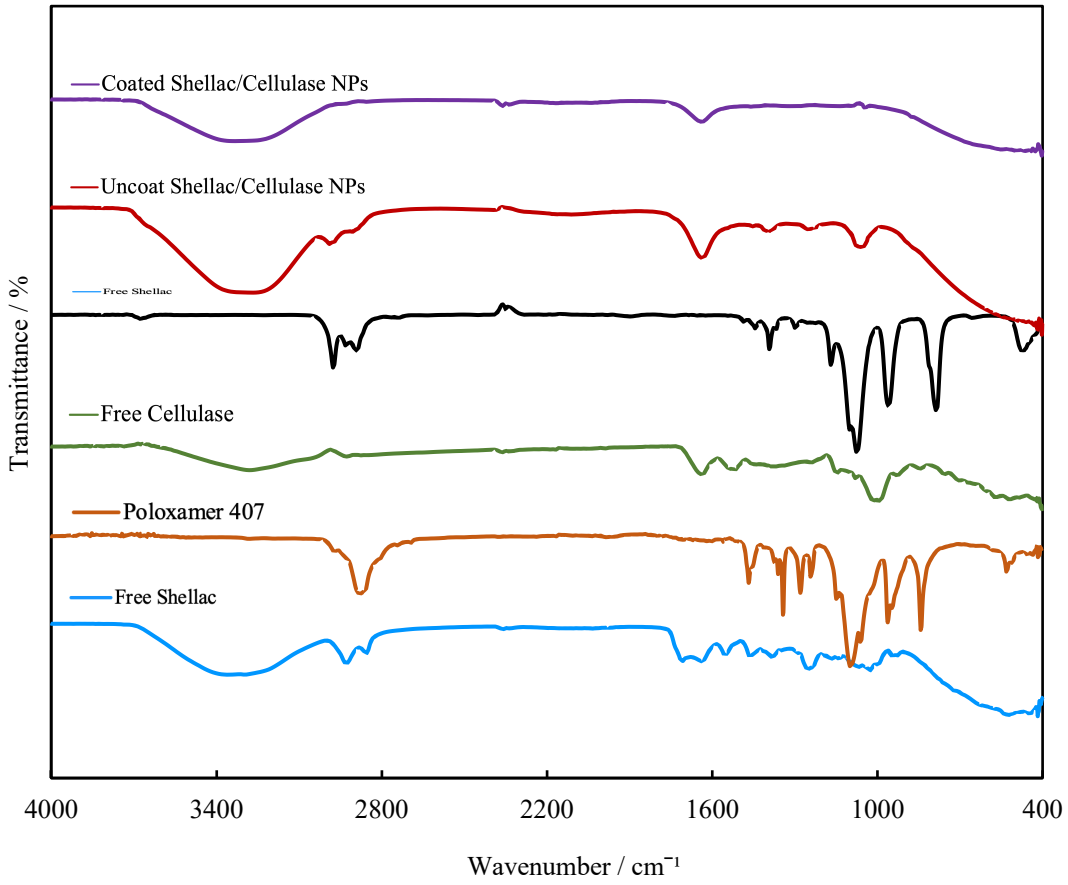

Figure 18. FT-IR spectra of free shellac, free P407, free cellulase, free TEOS, uncoated Cellulase-loaded shellac NPs, silica-coated Cellulase-loaded shellac NPs.

3.7. Encapsulation efficiency of enzymes in the shellac NPs

Encapsulation Efficiency (EE) is the percentage of enzyme successfully encapsulated in the nanoparticles. It is calculated using the formula below.

$$\text{Encapsulation Efficiency (EE)} = \frac{W_{theoretical} - W_{obtained}}{W_{theoretical}} \times 100\%,$$

Where $w_{theoretical}$ is the full weight of the added active agent (i.e., enzyme) while $w_{obtained}$ is the weight of the active agent actually encapsulated in the particles. EE of NPs at pH 4, which is the pH of the solution during the synthesis. The average EE of the enzymes in an uncoated shellac NPs at pH 4 is 89%±2%. For silica-coated shellac NPs at pH 4, EE is very similar, 91%±2%. At pH 4, the shellac is tightly packed and captures more efficiently the enzymes inside its core. The deposition of silica shell does not significantly change the EE.

3.8. Release Kinetics of uncoated and TEOS-coated shellac/enzyme NPs

Ideally, there is a need to centrifuge the particles out of the suspension to avoid scattering the light while reading the absorbance from the protein assay used to estimate the changes in the concentration of the enzyme released in the solution with time. However, the density of produced NPs turned out to be very close to the density of water. Therefore, it is hard to centrifuge such particles out of the aqueous suspension. To check the effect of the particles in the protein assay measurements, an additional check of scattering was done. It was found that it did not contribute strongly (a few %) to the overall absorbance of light. Therefore, the protein assay can be used without significant error without the centrifugation of the shellac NPs.

Release of encapsulated enzymes (Alcalase, Savinase, and Cellulase) is done at pH 7.5, the conditions of chronic wounds. The acidity of the chronic wounds varies from 7 up to 9 or even 10. Also, to assess the coated NPs, we use TEOS as a coating material rather than APTES because when adjusting pH to 7.5, APTES-coated NPs started to precipitate, and it becomes unsuitable for further experiments. Silica coated shellac NPs obtained by TEOS hydrolysis were stable and does not precipitate or aggregate under these conditions.

As the external stimulus to trigger the release of enzymes we chose the ultrasonic probe Branson 550 (Branson, USA). The ultrasonic probe used was 3mm titanium shaft which was

immersed in the container with the particle suspension (10 mL) and set to 10% of the sonicator maximum power which is 275 W for this probe. We used this setup to study the interaction of the US with the sample in the form of NPs suspension because the ultrasound is spread uniformly, and it is easier to adjust. It was anticipated that upon application of US, the silica shell will fracture, the core of shellac NPs starts to swell, and its matrix will disrupted which would facilitate the enzyme release in the aqueous phase. The enzyme concentration was monitored by using Bradford assay and standard calibration graphs. Figure 19 (A) illustrates that uncoated and TEOS-coated shellac/alcalase NPs without triggering with the US. The amount of released Alcalase is practically similar for both formulations (coated and uncoated). This can be explained with the high isoelectric point (IEP) of Alcalase, which is around 9, hence at pH 7.5 as it is positively charged as this pH is below the IEP. Shellac is always negatively charged, and in the process of co-precipitation, they electrostatically attract to each other. Therefore, it is harder for the NPs to release the corresponding enzyme with high IEP. Therefore, in this case silica coating does not significantly increase the release of Alcalase compared to the non-coated NPs. The amount of the released Alcalase falls within the range of 8±1%. Figure 19 (B) shows the release of Alcalase from uncoated and silica-coated shellac NPs after the application of the US. Immediately after sonication, the uncoated NPs release 13±2% of the Alcalase while the silica-coated NPs release only 8±0.4%, which is more preferable due to the more sustained release. Also, coated NPs demonstrate a lower amount of the released Alcalase due to the slow release. After 1 hour, the released Alcalase increased from 8±0.4% to 12±1%.

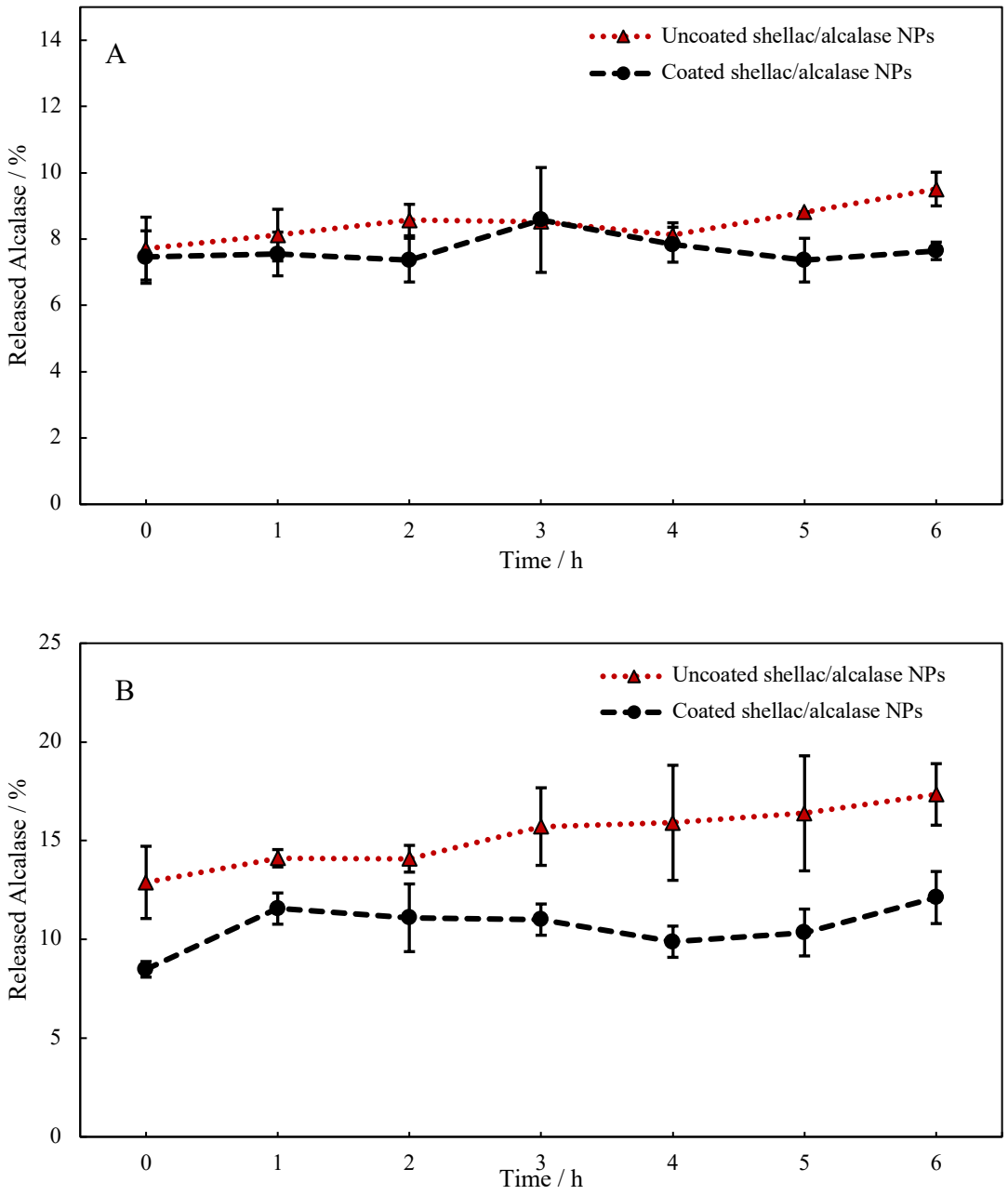

Figure 19. Release of Alcalase from (A) uncoated and silica-coated shellac/alcalase NPs (A) without application of US, and (B) After application of US.

Figure 20(A) shows the release of Savinase without application of US. Savinase has an IEP of around 9, which possesses a positive charge below IEP. However, silica coated NPs in this case have higher Savinase release than uncoated NPs. Possible explanation for this process is that the fracturing of the silica shell may cause stronger disruption of the cores and structural alterations induced by the US application compared with the case without the protective TEOS

coating. Uncoated NPs have a stable release from 8 to 9% within 6 hours. However, coated NPs release 10±1% of Savinase in the first hours, slowly increasing to 12±1%. According to Figure 20 (B), which demonstrates the release under the US usage, coated NPs show higher release from 23±1% up to 29±1% within 6 hours. A possible explanation for this process is that there is a fracturing of the silica shell that enhances the release of Savinase from the shellac NPs core. Also, silica can adsorb the released Savinase and serve as an additional source of released Savinase.

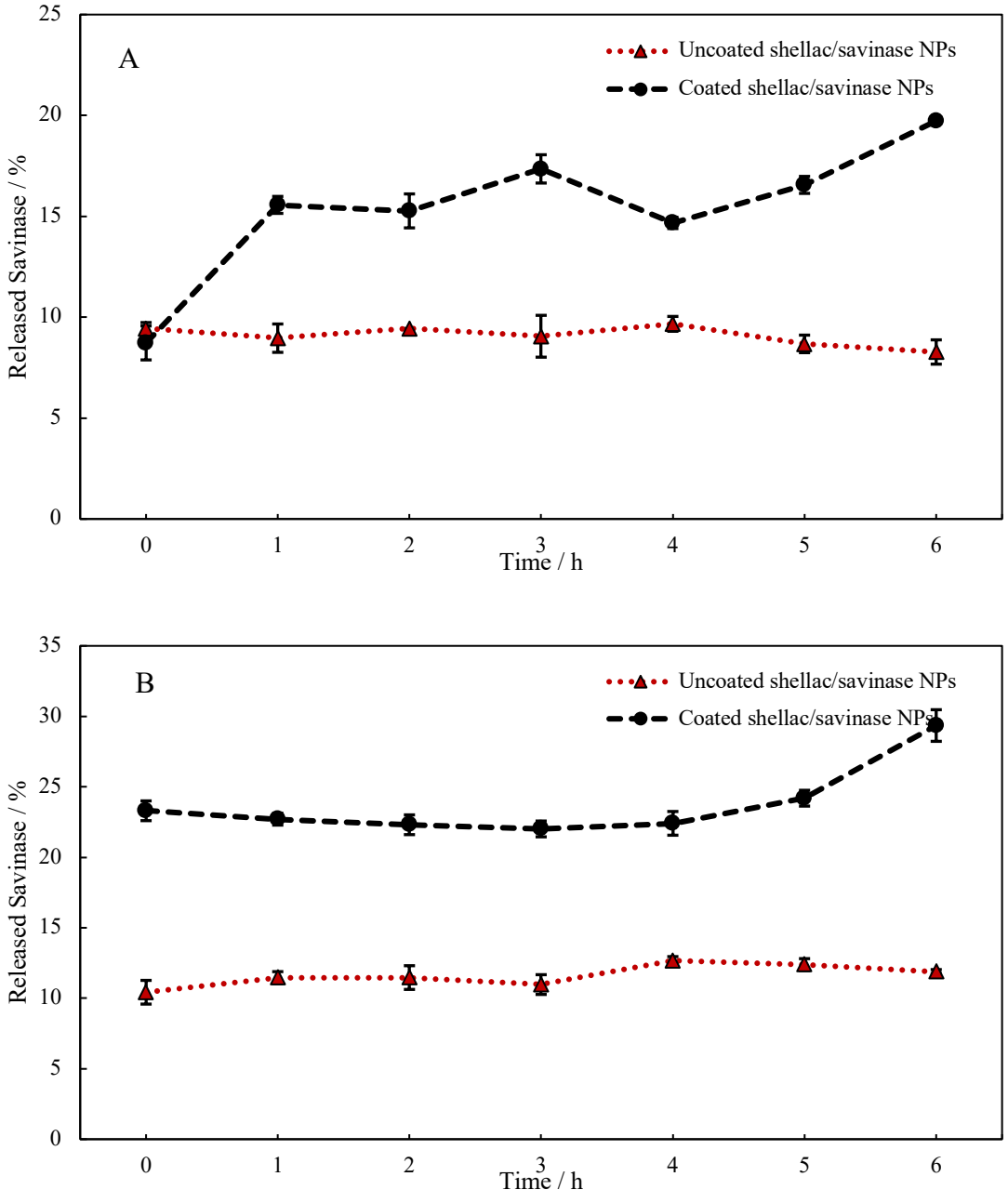

Figure 20. Release of Savinase from (A) uncoated and silica-coated shellac/Savinase NPs (A) without application of US, and (B) After application of US.

Figure 21 (A) shows the released amount of Cellulase without US usage. It indicates that uncoated NPs have a higher release from the beginning, which is 13±1% and it increases up to 15±1% within 6 hours since the start of the release experiment. Contrariwise to uncoated NPs, coated NPs demonstrate lower release at the beginning which is 6±1% then it starts to increase after 1 hour up to 12±1%. Further growth is shown from 1 hour to 6 hours. At 6 hours, it becomes slightly higher than the Cellulase release from the uncoated shellac NPs and equals to 16±0.4%. Figure 21 (B) shows the released amount of cellulase under the application of the US. Within 1-hour, uncoated NPs illustrate released cellulase of 14±0.2% and coated NPs 10±1%. Such differences show that TEOS serves as a barrier to the NPs and prevents them from leaching the enzyme. The release for uncoated NPs is relatively stable and does not change within 6 hours. While coated NPs after 1 hour start to release more cellulase that equals to 17±1% for 3 hours. At 4 hours it equals to 18±2%, at 5 hours 19±0.4%, at 6 hours 20±3%. Such high releases can be attributed to the low cellulase IEP which is about 5. Above its IEP (e.g., at pH 7.5 which is the pH of the experiment), the Cellulase has a negative charge that repels from the negatively charged shelloic acids of the matrix of the NPs core, hence it is release more easily than Alcalase or Savinase, which favorably electrostatically interact with shellac matrix.

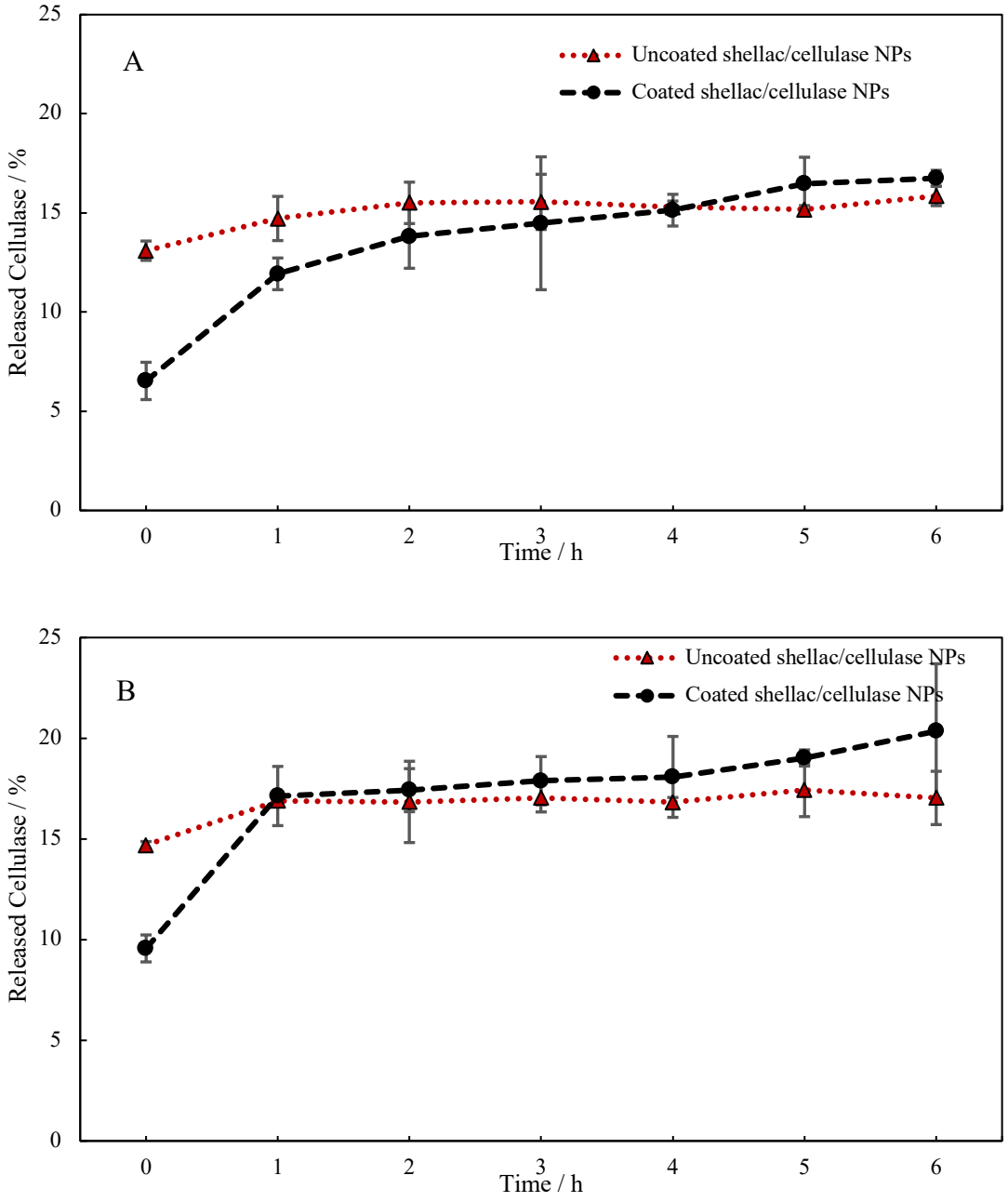

Figure 21. Release of Cellulase from (A) uncoated and silica-coated shellac/ Cellulase NPs (A) without application of US, and (B) After application of US.

3.9. Bacterial Biofilm Quantification

In order to assess the formulated and synthesized NPs on the bacterial biofilms, we chose *S. epidermidis* bacteria strain because it is prevalent in chronic wounds. The active component of NPs, which are enzymes that contribute to degrading the EPS of bacteria. Alcalase and Savinase can destroy proteins that are a major component of EPS. Cellulase

targets polysaccharides which are constituting the glycans found in EPS. In this experiment, we use medical ultrasound (Meishida Professional IB-5002, China) because we aim to disrupt the bacterial biofilm, and our NPs are located on the surface of the Petri dishes that are treated with the bacteria.

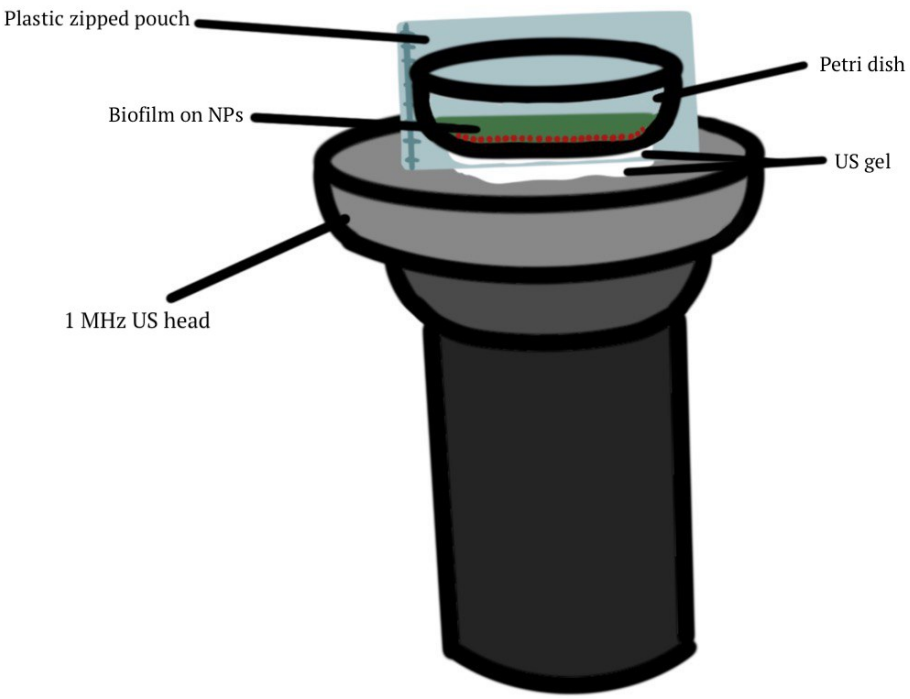

Scheme 6. Triggering of bacterial biofilm treated with NPs using 1 MHz US head.

Prior to the usage of NPs, we assess the US power and duration to avoid the contribution of the US to the disruption of biofilm solely from it. We tested two different powers, 40 kHz and 1 MHz of ultrasonic heads. Figure 22 demonstrates the calibration of 40 kHz medical US head. It is clearly shown that the cavitation induced by 40 kHz sonic head significantly eradicate the bacterial biofilm. Lower frequency sonic waves, such as 40 kHz, may have superior penetration and degradation abilities alone enabling cavitation to deeper levels of the biofilm and produce a larger degradation impact. The results in Figure indicate that the 40kHz sonic head is too abrasive for the biofilms alone and does not allow us to evaluate the effect of the enzyme-loaded NPs as there is too low residual amount of biofilm left even without NPs

treatment. Hence, we focused on using the US head of 1MHz whose calibration is presented in Figure 23.

Figure 22 shows the results of the NPs treatment on *S. epidermidis* biofilm. After calibration, we used NPs along with US.

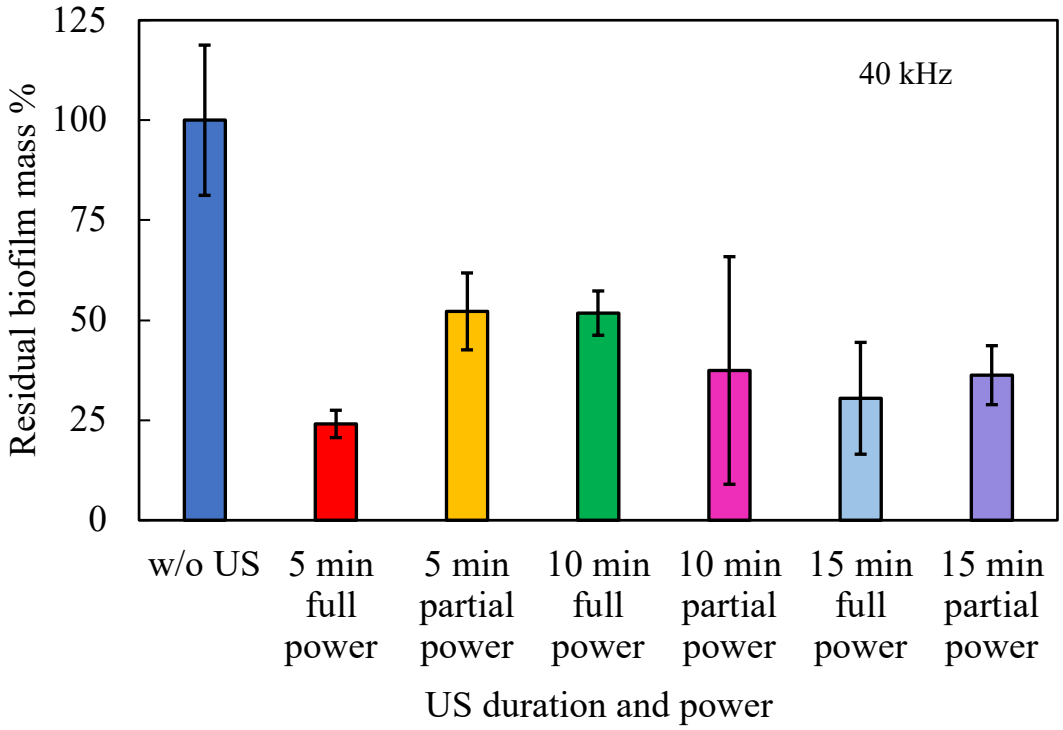

Figure 22. Residual biofilm mass (%) of *S. epidermidis* on non-treated plastics after 40kHz sonication. Full (partial) power is 30W (15W) for the 40kHz head.

The sonicator head at 1MHz has lower maximal power and cause less degradation to the biofilm alone. This absorption can restrict the ultrasonic energy's depth of penetration into the biofilm structure. Figure 23 shows that sonication with 1MHz alone does not have such a significant impact on the degradation of the biofilms compared to sonication at 40 kHz power. Therefore, for further experiments with NPs we used 1 MHz 5 min partial power.

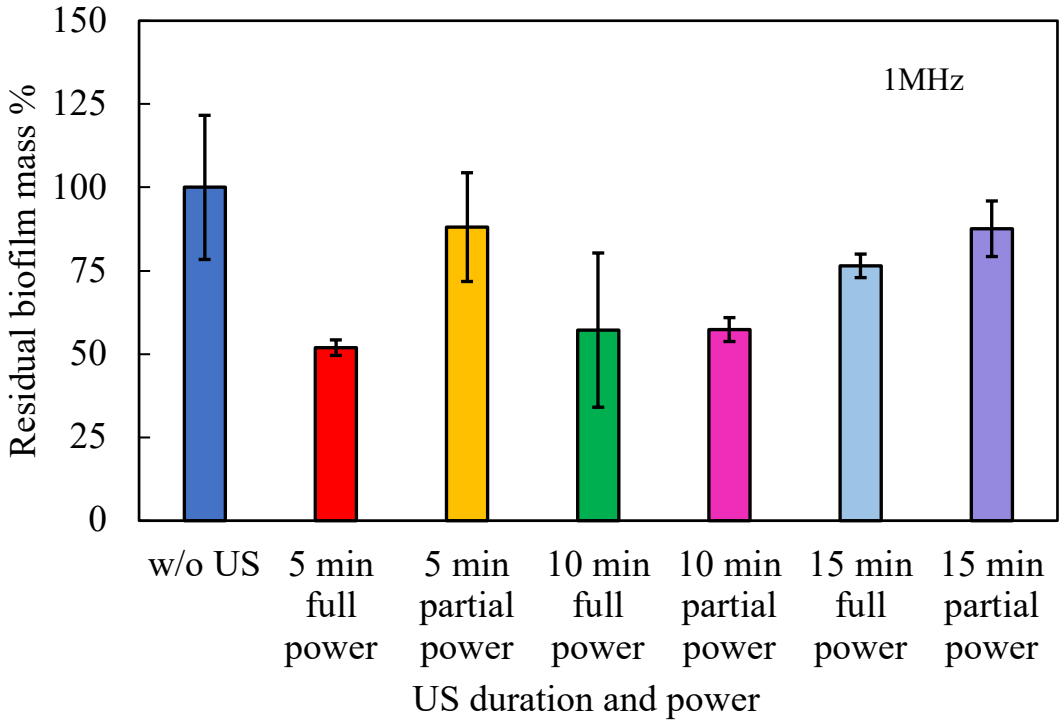

Figure 23. Residual biofilm mass (%) of *S. epidermidis* on non-treated plastics after 1MHz sonication. Full (partial) power in US mode is 3W (1.5W).

Figure 24 demonstrates the residual biofilm mass (%) after treating *S. epidermidis* bacterial biofilm with NPs. For the following treatments, we performed a t-test to check the statistical significance of the differences. In this experiment, bacteria without US (purple bar) plays the role of control. Also, we performed treatment of the uncoated unloaded with and without US (blue bars) to investigate the effect on the biofilm growth. According to the results, they do not suppress biofilm development. Comparing uncoated unloaded with coated unloaded NPs, there is a statistical significance between them where coated unloaded NPs produce a considerable suppression of the biofilm. This is probably due to the anti-adhesive abilities of the silica surfaces that have been reported, which leads to a decreased ability of *S. epidermidis* bacteria to attach to the surface and form a biofilm. Silica-coated NPs make the environment less suitable for bacterial adhesion, thus reducing biofilm development.

The residual biofilm mass for the uncoated Alcalase-loaded NPs (red bar) is 40%, while for the silica-coated Alcalase-loaded NPs (red bar) it is even less, around 25% and there is a

statistical significance between them. Due to the presence of Alcalase the EPS of biofilm is destroyed, and it is more enhanced after silica coating due to the synergetic effect between fracturing of coat and the release of active components onto the biofilm. Comparing the results for the release kinetics with Alcalase-loaded NPs, after 2 hours, the released amount of Alcalase is 12% for coated NPs.

There was no statistical significance for uncoated and silica-coated Cellulase-loaded NPs (green bars). It shows a considerable decrease in the residual biofilm mass and correlates with the release kinetics that was the most effective with these formulations. The release for uncoated and coated cellulase-loaded NPs showed an almost similar amount of release active component. It is due to the positive charge of cellulase and the easiest detachment from the negatively charged shellac matrix.

There is statistical significance between formulations for the uncoated and silica-coated Savinase-loaded NPs (yellow bars). Uncoated Savinase-loaded NPs show the least effect on biofilm eradication among the loaded NPs due to the lower release of Savinase in uncoated NPs, which is equal to 9% and it is relatively low. However, silica-coated Savinase-loaded NPs have more effective biofilm elimination due to the high release of Savinase, which is 16%.

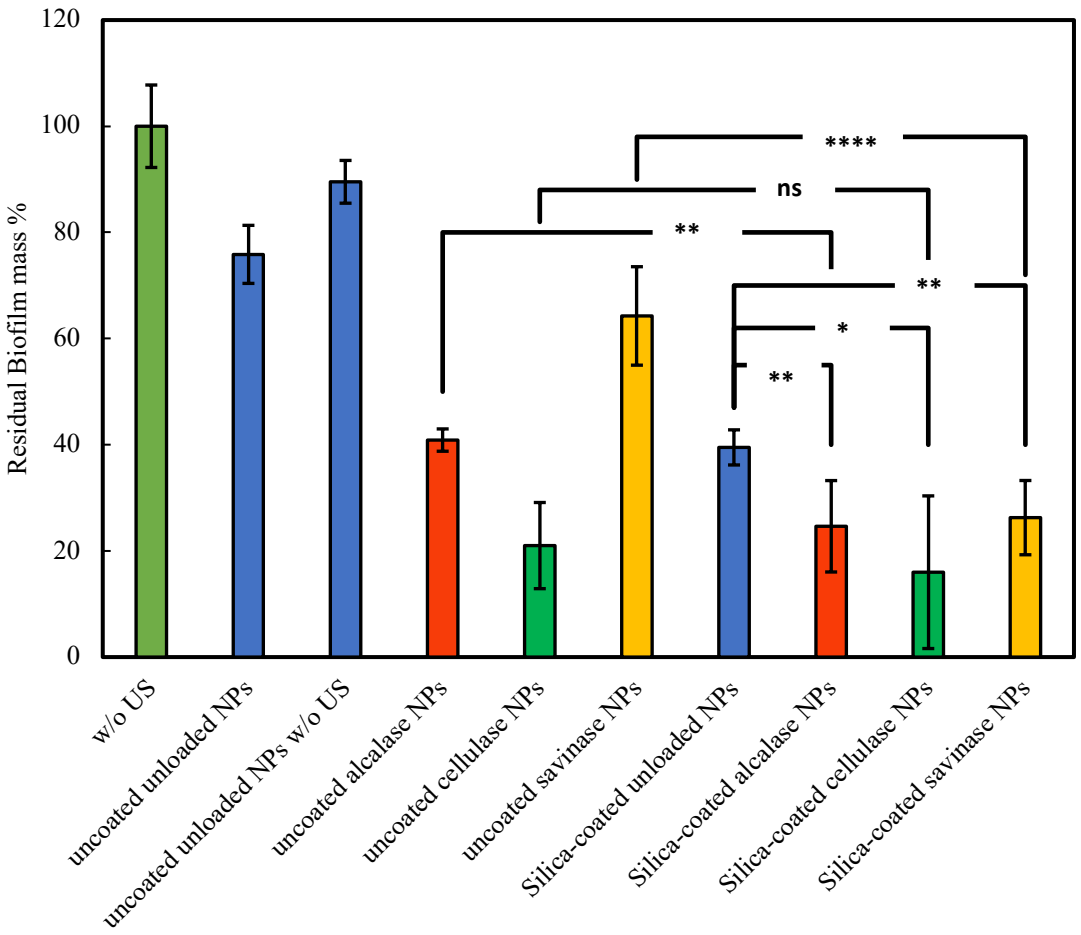

Figure 24. NPs treatments on *S. epidermidis biofilm* with and without US at 1MHz. The asterisks are for following statistical significances: *; $p < 0.05$, **; $p < 0.01$, ***; $p < 0.001$, ****; $p < 0.0001$, ns; not significant.

3.10. Cytotoxicity assay, PI, DAPI, and Hoechst dying for HeLa cells

We conducted a cytotoxicity test to assess the possible negative effects, including cell damage or death under the usage of NPs on the cells. MTS assay is used to check cell viability. It is based on the decrease of the tetrazolium by the examined cells to form a formazan dye which is colored and soluble in the media. As a proxy for human cells, we use HeLa cell line, that are cervical cancer cells which are immortalized and derived from adenocarcinoma or cervix. We chose this type of cells because it is highly proliferative and has a fast-doubling time which allowed us to conduct the experiments within the time allocated for the MSc thesis.

The bar graph in Figure 25 shows the cell viability after treating HeLa cells with uncoated unloaded shellac NPs, uncoated Cellulase-loaded shellac NPs, silica-coated unloaded shellac NPs, and silica-coated Cellulase loaded NPs. The most toxic for the cells are the concentrations 1:1 of NPs with media. The cell viability decreases when exposed to the uncoated Cellulase-loaded shellac NPs and TEOS-coated Cellulase-loaded shellac NPs. HeLa cells have a pH that is around 7 to 7.4, closer to physiological pH. However, our NPs have a pH of 4, which can significantly impact the behavior of cells at the stage of mixing. Exposing HeLa cells to the NPs of acidic pH can result in decreased cell viability. Also, acidic conditions of NPs can lead to ion imbalance within the cells. Moreover, calcium, potassium, and sodium ions that maintain cellular function can interfere with the acidic pH. It leads to disrupted ion homeostasis, which leads to cellular dysfunction. Generally, cellulase is considered safe and non-toxic to the cells. Also, its pH is neutral, therefore, it does not harm the cells.

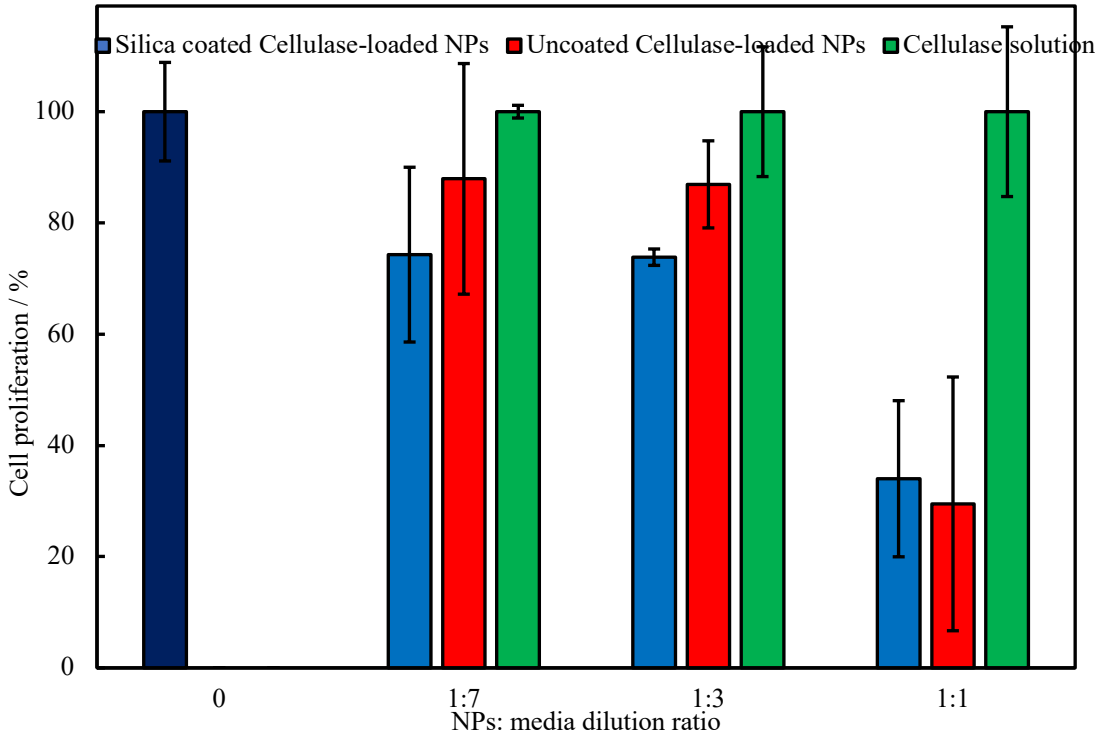

Figure 25. Cell proliferation (%) for HeLa cells treated with 0.1% TEOS-coated Cellulase-loaded shellac NPs, uncoated 0.03365wt% Cellulase-loaded shellac NPs, silica-coated unloaded shellac NPs (by using 0.1% TEOS), and uncoated unloaded shellac NPs.

The same trend is illustrated in Figures 26 and 27. Also, for coated unloaded shellac NPs and uncoated unloaded shellac NPs, the cell viability in a 1:1 ratio is somewhat less than the control.

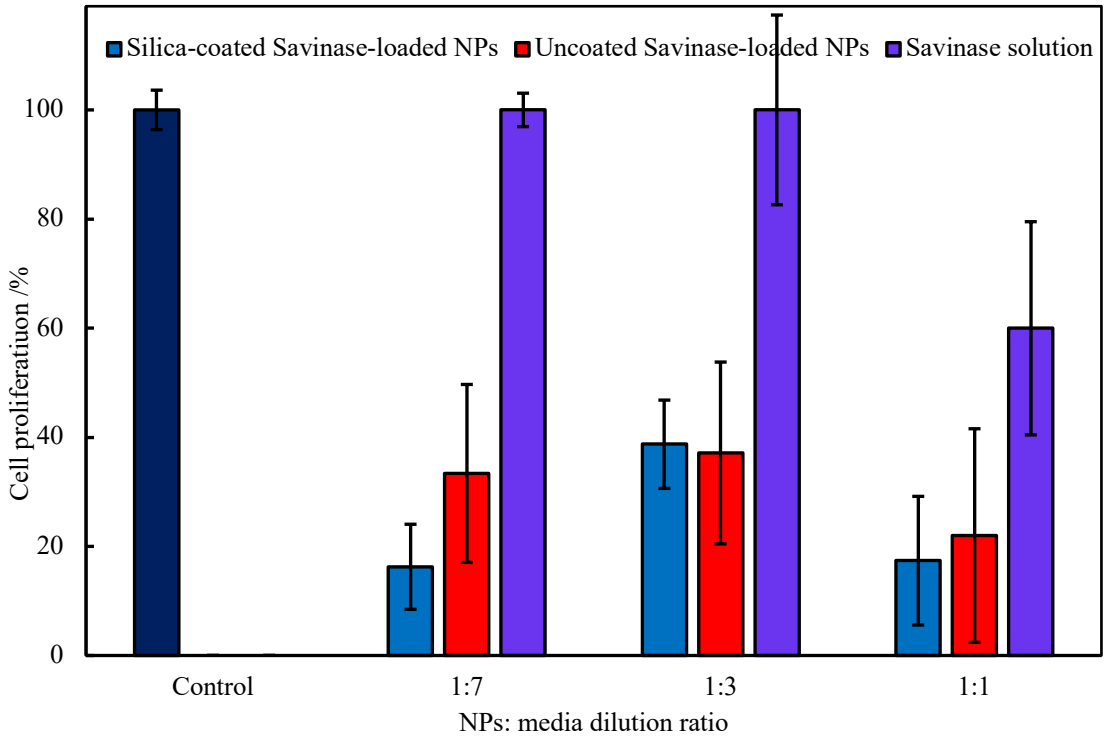

Figure 26. Cell proliferation (%) for HeLa cells treated with 0.1% TEOS-coated Savinase -loaded shellac NPs, uncoated 0.03365wt% Savinase-loaded shellac NPs, 0.1% silica-coated unloaded shellac NPs, and uncoated unloaded shellac NPs.

According to Figure 27, the most cytotoxic NP formulation is silica-coated Alcalase-loaded NPs (blue bar). NPs that contain silica have been shown to be cytotoxic to a variety of cell types, including HeLa cells. Therefore, the presence of silica may cause cellular stress, DNA damage, or disruption of cellular processes, ultimately resulting in cytotoxicity.

The uncoated Alcalase-loaded NPs (red bar) have erratic results because the 1:7 ratio shows the highest cytotoxicity. Possibly, it can happen because of some experimental error. This can be applied to the coated unloaded NPs (brown bar) in 1:3 ratio.

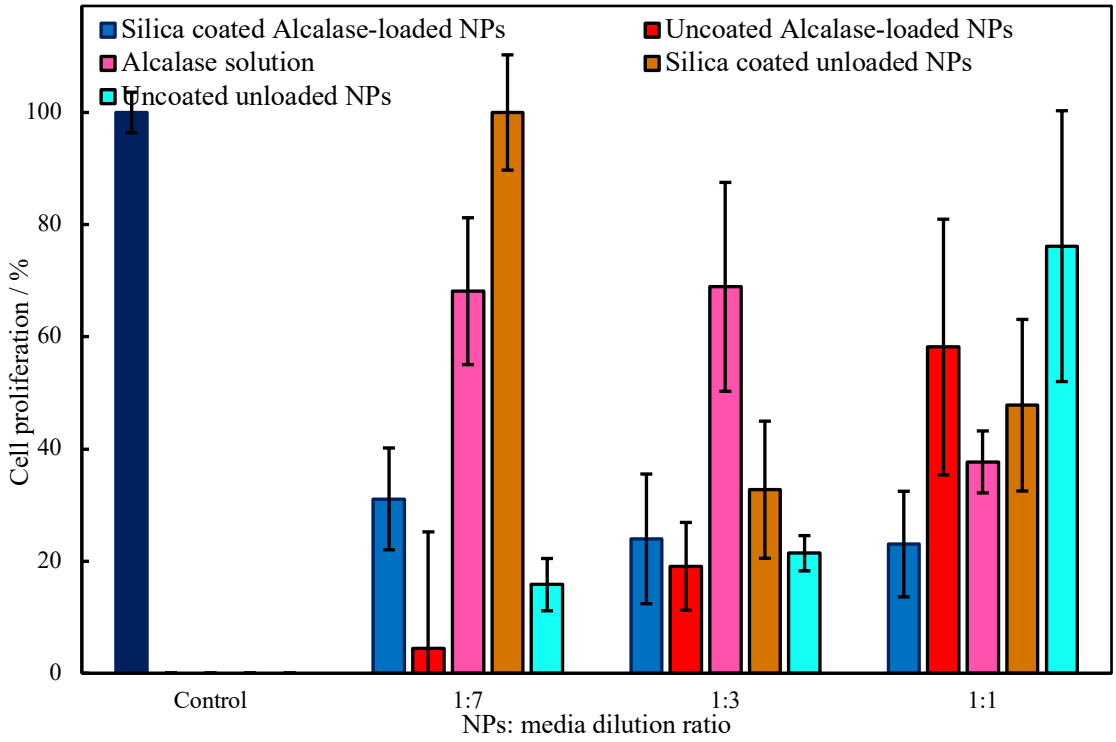

Figure 27. Cell proliferation (%) for HeLa cells treated silica-coated Alcalase -loaded shellac NPs (by 0.1wt% TEOS), uncoated 0.03365wt% Alcalase-loaded shellac NPs, silica-coated unloaded shellac NPs, and uncoated unloaded shellac NPs.

We also conducted DAPI/PI staining of the HeLa cells. DAPI is a blue fluorescent dye that binds to DNA and produces blue fluorescence when it is intercalated in its major grove. Another dye PI is a red fluorescent dye that may infiltrate cells with reduced membrane integrity, such as dead or injured cells, and selectively stain them. Although PI also binds to nucleic acids and turns fluorescent, it cannot pass through intact cell membranes.

According to Figure 28, silica-coated Alcalase-loaded NPs have increased dead cell percentage compared to control in a 1:3 ratio and 1:7 ratio, while silica-coated Savinase-loaded

NPs have a higher percentage of dead cells in a 1:7 ratio. It can occur due to the changes of the osmolarity effects that contribute to the higher death cell percentage.

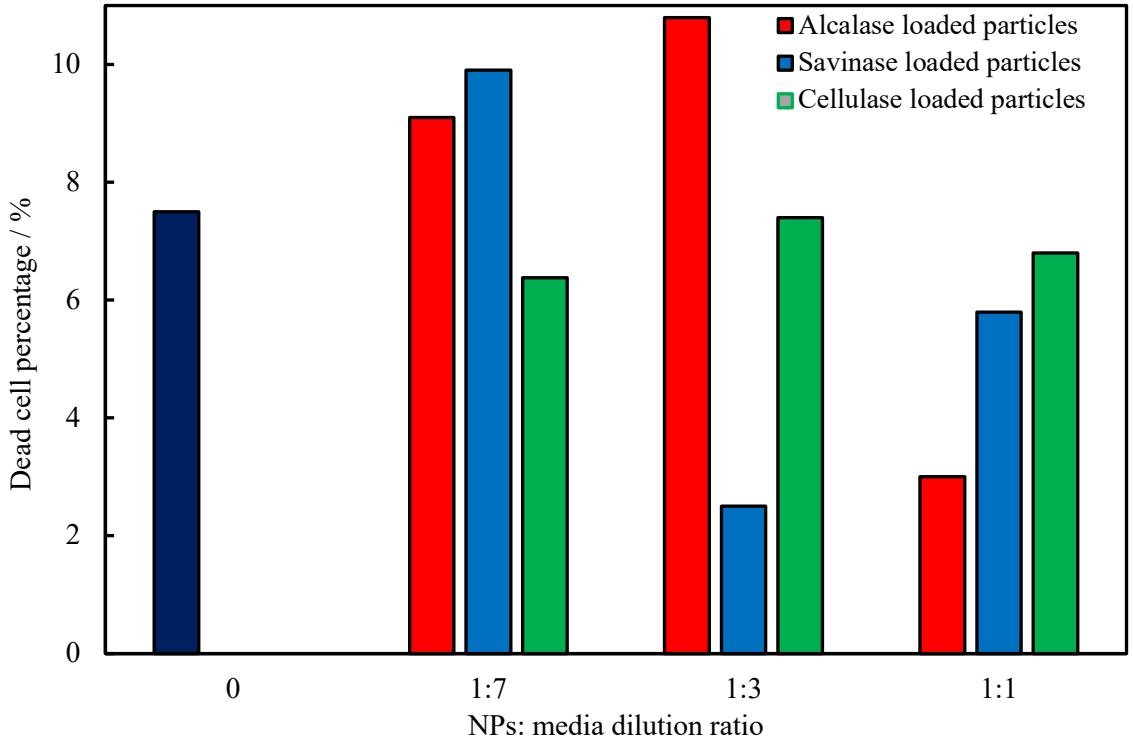

Figure 28. The percentage of dead cells based on double staining with DAPI and PI dyes for NPs coated with silica (from 0.1% TEOS precursor) and loaded with Alcalase, Savinase, and Cellulase.

4 Materials and Methods

Materials

Shellac ammonia salt (liquid) – 0.25wt% (SSB Aqua Gold, Germany), Poloxamer 407 (powder) – 0.25wt% (Sigma Aldrich, USA), Alcalase (liquid) – 0.3wt% (Merck KGaA, Germany), Savinase (liquid) – 0.3wt% (Novozymes, Denmark), Cellulase (powder) – 0.3wt% (Carolina, USA), HCl – 0.25 M, NaOH – 0.25 M, Bradford Assay – 1X (ThermoFisher Scientific, USA), APTES (3-Aminopropyl)triethoxysilane (liquid) – 0.2% (Sigma Aldrich, USA), TEOS tetraethyl orthosilicate (liquid) – 0.2% (Sigma Aldrich, USA), HeLa cells, CellTiter 96® Aqueous One Solution ReagentTM (Promega, UK), DAPI – 5µg/mL (Santa Cruz Biotechnology, Inc., USA), PI – 5µg/mL (Sigma Aldrich, USA), *S. epidermidis,* Crystal Violet – 0.1 % (Carolina, USA).

Equipment

pH-meter (Metler Toledo, USA), Laboratory Balances (Sartorius, Germany), Magnetic Stirrer with Hot Plate (ISOLAB, Germany), MiniSpin Centrifuge (Eppendorf, Germany), Litesizer 500 (Anton Paar, Austria), FLUOstar Omega (BMG LABTECH, Germany), Transmission Electron Microscopy (TEM JEOL JEM 1400 Plus, Japan), Scanning Electron Microscopy (ZEISS Crossbeam 540, Germany), Scanning Electron Microscope (JEOL JSM-IT200 LA, Japan), Ultrasonic Probe (Branson, USA), Medical Ultrasound (Meishida Professional IB-5002, China), Plasma Cleaner (Harrick Plasma, USA), Fluorescence microscope OLYMPUS CKX53SF (Evident Europe GmbH, Germany), Eppendorf centrifuge 5430 (Eppendorf, Germany), Cellometer K2 Cell Counter (Nexcelom, USA), Class II Microbiological Safety Cabinet (Euroclone, Italy), S41i CO_2 Incubator Shaker (Eppendorf New Brunswick, Germany), FT-IR spectroscopy (Thermo Scientific Nicolet iS10 FT-IR Spectrometer, USA).

4.1. Preparation and functionalization of Alcalase-loaded Shellac nanoparticles

The current methodology represents the “one pot” synthesis that enables the encapsulation of enzyme at a high pH of 10, to allow the Shellac to swell. The next step is to develop a Shellac core simultaneously precipitating the fixed ratio of Shellac ammonia salt and Poloxamer 407, which is 0.125wt%:0.125wt% respectively, while Alcalase with different concentrations together at pH 4 adding 0.25 M HCl dropwise. Shellac contracts and creates a core with the loaded enzyme in acidic conditions. It is the process of co-precipitation. The structure of Shellac and Poloxamer 407 are shown in Figure 30.

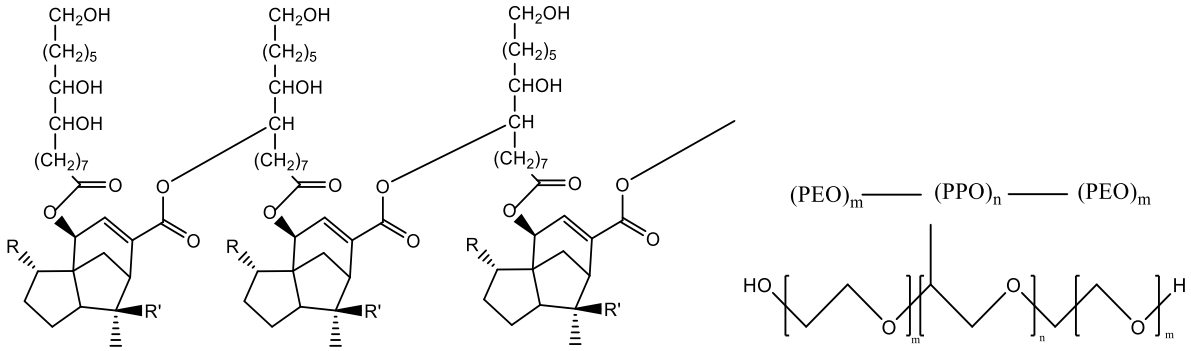

Figure 29. Shellac and Poloxamer 407 structure.

4.2. Shellac nanoparticles size, zeta-potential, and morphology characterization

The particle size and zeta potential of the Shellac NPs are measured by dynamic light scattering (DLS) using a Litesizer500 (Anton Paar, Austria). Transmission electron microscopy TEM (JEOL JEM 1400 Plus, Japan) performed a morphological examination of the NPs. For TEM, 10 μL of the sample was placed on carbon-coated copper grids and dried. Also, NPs for SEM imaging (JEOL JSM-IT200 LA, Japan) are prepared on the plastic slide 2x2 cm.

4.3. Coating of Shellac nanoparticles with silica precursors

After the encapsulation with Alcalase and the creation of the Shellac core stabilized by Poloxamer 407, there is a need to avoid the uncontrolled leaching of Alcalase. To achieve controlled release under the triggering by ultrasound, the deposition of a silica shell is considered an effective variant because it serves as a coating of the Shellac nanoparticles. As

organosilica precursors, (3-Aminopropyl) triethoxysilane APTES concentration of 0.2 wt% was used. The current methodology utilizes acid-catalyzed silica precursor hydrolysis to deposit a silica shell on the Shellac-enzyme composite nanoparticles.

4.3.1. APTES coating (organosilica)

APTES does not require adding ethanol to the synthesis process because it can be dissolved in water. Aminopropyl alkoxysilanes are frequently employed as coupling agents due to their bifunctionality. Their usage in aqueous media has advanced due to surface chemistry's growing importance in the life and environmental sciences. Unique characteristics of amino silanes are provided by the presence of amine functionality. The amine groups can catalyze the interaction between silane molecules and surface silanol groups to create siloxane bonds intra- or intermolecularly. Aminoalkoxysilanes are more reactive toward water than alkyl alkoxysilanes, and this increased reactivity makes aminoalkoxysilanes more likely to polymerize or oligomerize in solution spontaneously.

To produce the coating, mix 5 mL of 0.25 wt% Shellac ammonia salt with 5 mL of 0.25 wt% Poloxamer 407 in a 1:1 ratio. The concentration of the Shellac nanoparticles is 0.125wt%/0.125wt%. Increase pH to 10 using 0.25M NaOH in constant mixing. After, using 0.25M HCl drop pH to 5.

APTES solution should be prepared through dilution of 42 µL of APTES in 10 mL of water. The concentration of solution was 0.4 wt% APTES.

In the stage of coating, mix 10 mL of Shellac NPs (0.125wt%/0.125wt%) with 10 mL of 0.4 wt% APTES in 1:1 ratio. Final concentration of Shellac NPs is 0.0625wt%/0.0625wt% and APTES is 0.2 wt%. Adjust pH to 3 adding 0.25 M HCl in constant mixing and 55°C. Through observations, hydrolysis is successful at high temperature, and it starts to hydrolyze quicker than at ambient temperature. The structure of APTES is shown in Figure 31.

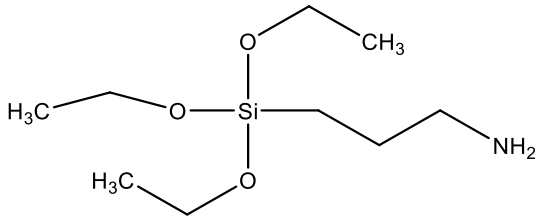

Figure 30. APTES structure.

4.3.2. TEOS coating (silica)

For the development of the TEOS-based silica coat, there is a need for EtOH in the solution because this type of silica precursor is hydrophobic and requires another suitable solvent rather than water. We used 10% EtOH because higher concentrations of ethanol would possibly dissolve shellac as it is soluble in higher ethanol concentrations in water. Also, the coating process is done under acidic conditions because shellac is soluble in an alkaline environment. Due to this fact, we do not use the convenient Stober method, as it requires higher pH supported by ammonia.

To coat the NPs with silica, we mix 5 mL of NPs 0.0625wt%/0.0625wt%/0.135wt% with 5 mL of 10% EtOH in 1:1 ratio. Final concentration of shellac NPs is 0.03125wt%/0.03125wt%/0.0675wt%. Then, add 10 mL of shellac NPs in 10% EtOH to 10 mL of 0.2 wt% TEOS in a 1:1 ratio. The final concentration of TEOS is 0.1 wt%, and shellac NPs is 0.0156wt%/0.0156wt%/0.03375wt%. Adjust pH to 4 adding 0.25M HCl in constant mixing at 55°C and at this temperature, the enzyme will not lose its activity.

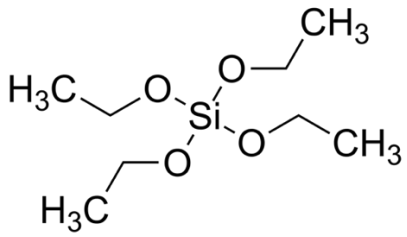

Figure 31. TEOS structure.

4.4. Encapsulation efficiency of Shellac/Alcalase NPs

To do the encapsulation efficiency of entrapped enzyme, there is a need to prepare the standard graph BSA concentrations need to be diluted from the stock solution of 0.4 mg/mL to 0.35, 0.3, 0.25, 0.2, 0.15, 0.1, 0.05 mg/mL in triplicates.

Mix 10 µL of standard concentrations of bovine serum albumin (BSA) with 300 µL of Bradford Assay (BA). Incubate for 10 min at room temperature and read the absorbance at 595 nm. Find the slope and use it in future calculations of encapsulation efficiency and release kinetics.

To assess the NPs, prepare it through the previously described method. Encapsulation efficiency needs to be done in NPs at pH 4.

4.5. Release Kinetics of Shellac/enzyme NPs

As in the encapsulation efficiency method, NPs were prepared at pH 4. After preparation and coating at pH 3 using APTES, adjust pH to 9. The release was then started. We monitor the suspension for 6 hours, and samples were taken and read after each hour. Do the readings of absorbance of BA after 10 min, 595 nm.

4.6. Bacterial Biofilm Quantification

4.6.1. Calibration of the medical US power and duration.

All bacterial work was done in a Class II Microbiological Safety Cabinet (Thermo Scientific, USA). A colony from stock *S. epidermidis* colonies on an agar plate was transferred into a 20 mL of nutrient broth (NB) in a sterile 50 mL tube for sonication and crystal violet (CV) assay overnight. The next day bacterial culture was adjusted to OD600=0.1 concentration in 96-well nunc plate on FLUOstar Omega plate reader (BMG LABTECH, Germany) at 600 nm, and 4mL was transferred to each Petri dish. The bacteria were incubated for 24 hours to form biofilms.

On day 3, all Petri dishes with planktonic cells except controls (- bacteria; - ultrasound) were put into packages with 2mL of diluted ultrasonic gel, zipped, and sonicated on 40kHz head with the application of additional 2mL of gel to medical ultrasound for 5, 10, 15 min at full and partial powers. The end time of US treatment was recorded and labeled on Petri caps.

After 2 hours, the fluids were discarded, and Petri dishes were dipped into a 600 mL beaker with deionized water (DI water) and washed gently with additional water from the caps of the Petri dishes. Then we let them dry for 15 minutes. Then 3 mL of CV was applied to Petri dishes and left for 40 minutes. After that, CV was poured into the trash beaker with bleach. Plates were washed with DI water in the big beakers (1 L and 600 mL) to remove the unbound CV. After drying, 30% acetic acid (3mL) was added to each plate, mixed, and left for 10 minutes. Then triplicates of 200 μL from each sample were transferred to a 96-well nunc (without lid) microplate, and the optical density was measured at 600 nm. The same procedure was repeated for the 1 MHz ultrasonic head.

4.6.2. Bacterial Biofilm Quantification after sonication with NPs using CV Assay

A colony from stock of *S. epidermidis* colonies on agar plate was transferred into a 20 mL of NB in a sterile 50mL tube for sonication and crystal violet assay overnight. 3mL of nanoparticles (silica-coated unloaded shellac NPs, silica-coated Alcalase-loaded shellac NPs, silica-coated Cellulase-loaded shellac NPs, TEOS-coated Savinase-loaded shellac NPs, uncoated unloaded shellac NPs, uncoated Alcalase-loaded shellac NPs, uncoated Cellulase-loaded shellac NPs, uncoated Savinase-loaded shellac NPs) were poured to the plasma cleaned (for 6 min) and poly-l-lysine (5 mg diluted in 5mL DI H_2O) coated Petri dishes and kept there for 5 minutes with their further removal and drying of Petri dishes, followed by UV-sterilization (5 min). Controls also had plasma cleaned and poly-lysine coated plates. The next day bacterial culture was adjusted to OD600=0.1 concentration in nunc 96 well plate on FLUOstar Omega (BMG LABTECH, Germany) plate reader at 600 nm, and 3mL was

transferred to each NP treated and non-treated (control) Petri dishes. The bacteria were incubated for 24 hours to form biofilms on pretreated plates. On day 3, all Petri dishes with planktonic cells except controls (- bacteria; - ultrasound) were put into packages with 2mL of diluted ultrasonic gel, zipped, and sonicated on 1 MHz head with the application of additional 2mL of gel to medical ultrasound for 5 minutes partial powers. The end time of US treatment was recorded and labeled on petri caps. The US head was wiped each time, and 2mL of gel was reapplied for each plate. After 2 hours, the fluids were discarded, and plates were dipped into a 600 mL beaker with deionized water (DI water) and washed gently with additional water from the caps of Petri dishes. Then we let them dry for 15 minutes. Then 3 mL of CV was applied on Petri dishes and left for 40 minutes. After that, crystal violet was poured off into the trash beaker with bleach, plates were washed with DI water in the big beakers (1 L and 600 mL) to remove the unbound CV. After drying, 3 mL of 30% acetic acid was added to each plate and mixed, and left for 10 minutes. Then triplicates of 200 µL from each sample were transferred to a 96-well nunc (without lid) microplate, and the optical density was measured at 600 nm.

4.7. Cytotoxicity assay, PI, DAPI, and Hoechst dying for HeLa cells

HeLa cells were cultured in DMEM supplemented with 10% FBS and 1% L-glutamine under humidified conditions at 37 °C, 5% CO_2 in T75 flasks until a confluency of 80% was achieved, determined by visualization with an optical microscope. Passaging was done at 80% confluency to ensure that the cells remained in the exponential phase for experimentation.

Passaging was performed by aspirating old media, washing with PBS, and incubating with 1× trypsin EDTA at 37 °C 5% CO_2 for 5 min until the cells were detached in suspension. The trypsin was then neutralized with completed DMEM at a 1:1 volumetric ratio and gently centrifuged at 400 rpm for 5 min, the supernatant was aspirated, and the pellet was resuspended in 9 mL of completed DMEM.

Cells were counted and diluted to achieve 5 000 HeLa cells per 100 µL, which were seeded into a 96-well plate and incubated for 24 hours at 37 °C 5% CO_2.

The medium was then removed and replaced with fresh media for control wells and treatment solutions consisting of coated loaded, uncoated loaded particles with media at different ratios (1:7, 1:3, and 1:1). The particles solution was diluted with media solution and filtered through 0.22 µm filter in order to avoid contamination. The wells were washed with Glucose solution (5%) in order to remove debris from the media.

Treatments were performed in different dilutions, and each dilution was applied in 3-4 replicates.

After 24 hours of incubation at 37 °C, 5% CO_2, 20 µL of CellTiter 96® Aqueous One Solution ReagentTM (Promega, UK) were added and incubated for 2 hours under the same conditions listed above. The absorbance was then read at 492 nm. These data were calculated into cell count data using the Beer–Lambert extinction coefficient law using absorbance values from a fixed number of cells in media.

For PI staining take10 µL of working PI solution (5 µg/mL) were added and images obtained under fluorescence microscope. The DAPI staining: 10 µL of working DAPI solution (5µg/mL) were added and images obtained under fluorescence microscope.

5 Conclusion and Future Work

Bacterial biofilms that are accumulated in wounds and implants have a variety of unfavorable consequences for health, including slow and challenging wound healing, inflammation and rejection which leads to the removal of the implant. The leading cause of bacterial resistance is EPS which acts as a barrier in bacterial biofilms, protecting bacteria from antibacterial agents. Therefore, EPS is a central target of all the discussed methods. Once the EPS is removed, the medication starts the healing process of the wound.

Current biofilm therapies do not entirely eliminate microbial colonies or prevent growth, indicating that more comprehensive research is needed. Treatments based on nanotechnology are currently being investigated as a promising tool for medication delivery, combined treatment, and implant modifications. Ultrasound debridement, hydrogels, and recently developed nanotechnologies have potential in wound and implant therapy [2]. Additionally, the application of enzymes has the advantage of fast-healing wounds. However, the instability and improving their properties lead to additional costs, which is not beneficial.

Future prospects may include the development of gene therapy targeting microRNA. Also, targeting recombinant enzymes and hormones can help the wound repair process. However, apart from the advantages of current methods, both medical and surgical have many limitations, such as short residence time, low efficacy, high toxicity, high costs, and high risk of infection. Traditional wound care therapies, such as topical medications, wound dressings, and skin transplants, are ineffective in treating chronic wounds. These limitations have forced greater attention and investigation into the function of Complementary and Alternative Medicines (CAMs) in treating non-healing chronic wounds, which may give promising treatments in the near future. Additionally, 3D printed skin on the wound might be a potential approach. Understanding the mechanics of wound healing, wound microbiology, and existing

wound dressings might be highly beneficial to the medical and pharmaceutical communities in developing more effective wound dressings for particular individuals.

The presented research in this thesis includes Shellac NPs synthesis and their use for encapsulation with enzymes that have auspicious results for the long-term study of their effects on biofilms upon application of US triggered release. Also, the coating of Shellac NPs was performed with organosilica and silica precursors such as APTES and TEOS. However, the organosilica coating with APTES was not stable at neutral and alkaline conditions that are close to the pH of the chronic wounds due to colloidal stability issues. Therefore, in the future, this direction of protective coating will not be applicable and useful. However, TEOS coating with the encapsulated enzymes into the shellac core was also performed and was stable at the conditions of the experiment. TEM image analysis of silica coated shellac NPs indicate the uniform layers of the silica shell. SEM imaging also showed a consistent correlation between TEM and DLS particle size. Moreover, to prove that there are encapsulated enzymes in the shellac core and silica coating on the surface, EDS analysis and FT-IR spectroscopy were performed. Indeed, there is an indication of the presence of nitrogen and silica as an indication of enzymes and silica. Moreover, the release kinetics study showed the efficient and controlled leaching of enzymes under neutral pH. The most effective formulation in that matter was silica-coated Cellulase-loaded shellac NPs. To assess the effectiveness of these formulations, bacterial testing was conducted. Uncoated loaded and coated loaded NPs have shown success in the biofilm eradication that is correlated with the release kinetics study. Additionally, the cytotoxicity test showed that the formulations were moderately cytotoxic when they were exposed to the HeLa cells.

Future implementations of this study will include TEM imaging to see the shell thickness and how it will look in a cracked condition after applying US. Also, due to the precipitation of APTES-coated NPs at pH 7.5, to improve it using additional stabilizers. Then,

to introduce the NPs with neutral pH for cytotoxicity assessing cell viability. Also, in addition to the biofilm mass conduct the experiment with dying of bacteria to check the level and dead bacteria using AO or DAPI staining combined with PI. In addition, the metabolic activity of the biofilm can be assessed after the different treatments and application of US by using resazurin assay.

Consequently, more research is needed to understand biofilm dispersal mechanisms and enhance the synergy between dispersants and antibiotics to avoid the risk of spreading sepsis and infection, making dispersants a safe and effective tool in controlling infectious biofilms.

References

1. Crafts, T. S.; Gasparini, A.J.; Dantas, G. Next-Generation Approaches to Understand and Combat the Antibiotic Resistome. *Nat. Rev. Microbial.* **2017**, *15* (7), 422–434.

2. Tian, S.; van der Mei, H. C.; Ren, Y.; Busscher, H. J.; Shi, L. Recent Advances and Future Challenges in the Use of Nanoparticles for the Dispersal of Infectious Biofilms. *J. Mater. Sci. Technol.* **2021**, *84*, 208–218.

3. Dhar, Y.; Han, Y. Current Developments in Biofilm Treatments: Wound and Implant Infections. *Eng. Regener.* **2020**, *1*, 64–75.

4. Barroso, A.; Mestre, H.; Ascenso, A.; Simões, S.; Reis, C. Nanomaterials in Wound Healing: From Material Sciences to Wound Healing Applications. *Nano Select* **2020**, *1* (5), 443–460.

5. Chandi, R; Banthia, P.; Banthia, R. Biofilms: A Microbial Home, *J. Indian Soc. Periodontal.* **2011**, *15* (2), 111–114.

6. Davies D. Understanding Biofilm Resistance to Antibacterial Agents. *Nat. Rev. Drug Discov.* ***2003,*** 2 (2), 114–122.

7. Gajula, B.; Munnamgi, S.; Basu, S. How Bacterial Biofilms Affect Chronic Wound Healing. *Int. J. Surg: Global Health* **2020**, *3*(2), e16.

8. Di Martino, P. Extracellular Polymeric Substances, a Key Element in Understanding Biofilm Phenotype. *AIMS Microbiology* **2018**, *4* (2), 274–288.

9. Toyofuku, M.; Inaba, T.; Kiyokawa, T.; Obana, N.; Yawata, Y.; Nomura, N. Environmental Factors That Shape Biofilm Formation. *Biosci., Biotechnol., Biochem.* **2016**, *80* (1), 7–12.

10. Van Houdt, R.; Michiels, C. W. Role of Bacterial Cell Surface Structures in Escherichia Coli Biofilm Formation. *Research in Microbiology* **2005**, *156* (5-6), 626–633.

11. Stoodley, P.; Sauer, K.; Davies, D. G.; and Costerton, J. W. Biofilms as complex differentiated communities. *Annu. Rev. Microbiol*. **2002**, 56, 187–209.

12. Dunne, W. M. Jr. Bacterial adhesion: seen any good biofilms lately? *Clin. Microbiol. Rev.* **2002**, 15, 155–166.

13. Bogino, P. C., Oliva Mde, L., Sorroche, F. G., and Giordano, W. The role of bacterial biofilms and surface components in plant-bacterial associations. *Int. J. Mol. Sci.* **2013**, 14, 15838–15859.

14. Caruso, C.; Rizzo, C.; Mangano, S.; Poli, A.; Di Donato, P.; Finore, I. Production And Biotechnological Potential Of Extracellular Polymeric Substances From Sponge-Associated Antarctic Bacteria. *Appl. Environ. Microbiol.* **2018**, 84:e01624-17.

15. Khatoon, Z.; McTiernan, C.D.; Suuronen, E.J.; Mah, T.F.; Alarcon, E.I. Bacterial Biofilm Formation on Implantable Devices and Approaches to its Treatment and Prevention. *Heliyon* **2018**, 4(12), e01067.

16. Shokouhfard M.; Kermanshahi R. K.; Shahandashti R. V.; Feizabadi M. M.; Teimourian S. The inhibitory effect of a *Lactobacillus acidophilus* derived biosurfactant on biofilm producer *Serratia marcescens*. *Iran J. Basic Med. Sci.* **2015**, 18 1001–1007.

17. Pakharukova N.; Tuittila M.; Paavilainen S.; Malmi H.; Parilova O.; Teneberg S. Structural basis for *Acinetobacter baumannii* biofilm formation. *Proc. Natl. Acad. Sci. U.S.A.* **2018**, 115, 5558–5563.

18. Nadell, C. D.; Xavier, J. B.; Levin, S. A.; Foster. K. R. The Evolution Of Quorum Sensing In Bacterial Biofilms. *PLoS Biology* **2008**, 6, 171–179.

19. Annous B.A.; Fratamico P.M.; Smith J.L. Quorum Sensing In Biofilms: Why Bacteria Behave The Way They Do. *J. Food Sci*. **2009**, 74(1):R24–R37.

20. Dickschat J. S. Quorum Sensing And Bacterial Biofilms. *Nat. Prod. Rep.* **2010**, 27, 343–369.

21. Hannan, T. J.; Mysorekar, I. U.; Hung, C. S.; Isaacson-Schmid, M. L.; Hultgren, S. J. Early Severe Inflammatory Responses to Uropathogenic E. Coli Predispose to Chronic and Recurrent Urinary Tract Infection. *PLoS Pathogens* **2010**, *6* (8), e1001042.

22. Malone, M.; Bjarnsholt, T.; McBain, A.J. The Prevalence of Biofilms in Chronic Wounds: A Systematic Review and Meta-analysis of Published Data J. *Wound Care*, **2017**, 26 (1), 20–25.

23. Kataoka, Y.; Kunimitsu, M.; Nakagami, G.; Koudounas, S.; Weller, C. D.; Sanada, H. Effectiveness of Ultrasonic Debridement on Reduction of Bacteria and Biofilm in Patients with Chronic Wounds: A Scoping Review. *Int. Wound J.* **2020**, *18* (2), 176–186.

24. Percival, S.L.; Hill, K.E.; Malic, S.; Thomas, D.W.; Williams, D.W. Antimicrobial tolerance and the significance of persister cells in recalcitrant chronic wound biofilms. *Wound Repair Regen*. **2011**, *19*, 1–9.

25. Abushaheen, M. A.; Muzaheed; Fatani, A. J.; Alosaimi, M.; Mansy, W.; George, M.; Acharya, S.; Rathod, S.; Divakar, D. D.; Jhugroo, C.; Vellappally, S.; Khan, A. A.; Shaik, J.; Jhugroo, P. Antimicrobial Resistance, Mechanisms and Its Clinical Significance. *Disease-a-Month* **2020**, *66* (6), 100971.

26. Bi, Y.; Xia, G.; Shi, C.; Wan, J.; Liu, L.; Chen, Y.; Wu, Y.; Zhang, W.; Zhou, M.; He, H.; Liu, R. Therapeutic Strategies against Bacterial Biofilms. *Fundamental Research* **2021**, *1* (2), 193–212.

27. Yazdanpanah, L.; Nasiri, M.; Adarvishi, S. Literature Review On The Management Of Diabetic Foot Ulcer WJD 5 Th Anniversary Special Issues (4): Diabetes-Related Complications. *World J. Diabet*. **2015**, *6*, 37–53.

28. Shkodenko, L.; Kassirov, I.; Koshel, E. Metal Oxide Nanoparticles against Bacterial Biofilms: Perspectives and Limitations. *Microorganisms* **2020**, *8* (10), 1545.

29. Mohammad, S.; Mortazavi, J.; Darvish, L.; Abounajmi, M.; Zarei, S.; Zare, T., Taheri, M; Nematollahi, S. Alteration Of Bacterial Antibiotic Sensitivity After Short-Term Exposure To Diagnostic Ultrasound. *Iran Red Crescent Med. J.* **2015**, *17*: e26622.

30. Kalishwaralal, K.; BarathManiKanth, S.; Pandian, S. R. K.; Deepak, V.; Gurunathan, S. Silver Nanoparticles Impede the Biofilm Formation by Pseudomonas Aeruginosa and Staphylococcus Epidermidis. Colloids and Surfaces B: *Biointerfaces* **2010**, *79* (2), 340–344.

31. Avila-Rodríguez, M.; Meléndez-Martínez, D.; Licona-Cassani, C.; Aguilar-Yañez, J.; Benavides, J.; Sánchez, M. Practical Context of Enzymatic Treatment for Wound Healing: A Secreted Protease Approach (Review). *Biomed. Rep.* **2020**, *13* (1), 3–14.

32. Masri, S.; Zawani, M.; Zulkiflee, I.; Salleh, A.; Fadilah, N.I.M.; Maarof, M.; Wen, A.P.Y.; Duman, F.; Tabata, Y.; Aziz, I.A.; et al. Cellular Interaction of Human Skin Cells towards Natural Bioink via 3D-Bioprinting Technologies for Chronic Wound: A Comprehensive Review. *Int. J. Mol. Sci*. **2022**, *23*, 476.

33. Cooper, R.A.; Bjarnsholt, T.; Alhede, M. Biofilms In Wounds: A Review Of Present Knowledge. *J. Wound Care,* **2014***,* 23, 570–582.

34. Bi, Y.; Xia, G.; Shi, C.; Wan, J.; Liu, L.; Chen, Y.; Wu, Y.; Zhang, W.; Zhou, M.; He, H.; Liu, R. Therapeutic Strategies against Bacterial Biofilms. *Fundamental Research* **2021**, *1* (2), 193–212.

35. Jiang, W.; Wang, Y.; Tang, J.; Peng, J.; Wang, Y.; Guo, Q.; Guo, Z.; Li, P.; Xiao, B.; Zhang, J. Low-Intensity Pulsed Ultrasound Treatment Improved The Rate Of Autograft Peripheral Nerve Regeneration In Rat. *Sci. Rep.* **2016**, **6**: 22773.

36. Carding, S., Verbeke, K., Vipond, D.T., Corfe, B.M. and Owen, L.J. Dysbiosis Of The Gut Microbiota In Disease. *Microb. Ecol. Health Dis.* **2015**, *26*, 26191.

37. Kaiser P.; Wächter J.; Windbergs M. Therapy of infected wounds: overcoming clinical challenges by advanced drug delivery systems. *Drug Deliv Transl Res*., **2021**, *11*(4), 1545-1567.

38. Varier, K. M.; Gudeppu, M.; Chinnasamy, A.; Thangarajan, S.; Balasubramanian, J.; Li, Y.; Gajendran, B. Nanoparticles: Antimicrobial Applications and Its Prospects. *Advanced Nanostructured Materials for Environmental Remediation* **2019**, *25*, 321–355.

39. Newase, S.; Bankar, A. Synthesis Of Bio-Inspired Ag−Au Nanocomposite And Its Anti-Biofilm Efficacy. *Bull. Mater. Sci.* **2017**, *40*, 157−162.

40. Pang, S.; Gao, Y.; Wang, F.; Wang, Y.; Cao, M.; Zhang, W.; Liang, Y.; Song, M.; Jiang, G. Toxicity Of Silver Nanoparticles On Wound Healing: A Case Study Of Zebrafish Fin Regeneration Model. *Sci. Total Environ.*, **2020**, *717*, 137178.

41. Gao, L.; Fan, K.; Yan, X. Iron Oxide Nanozyme: A Multifunctional Enzyme Mimetic for Biomedical Applications. *Theranostics* **2017**, *7* (13), 3207–3227.

42. Kataoka, Y.; Kunimitsu, M.; Nakagami, G.; Koudounas, S.; Weller, C. D.; Sanada, H. Effectiveness of Ultrasonic Debridement on Reduction of Bacteria and Biofilm in Patients with Chronic Wounds: A Scoping Review. *Int. Wound J.* **2020**, *18* (2), 176–186.

43. Dhar, Y.; Han, Y. Current Developments in Biofilm Treatments: Wound and Implant Infections. *Eng. Regener.* **2020**, *1*, 64–75.

44. Casadidio, C.; Butini, M. E.; Trampuz, A.; Di Luca, M.; Censi, R.; Di Martino, P. Daptomycin-Loaded Biodegradable Thermosensitive Hydrogels Enhance Drug Stability and Foster Bactericidal Activity against Staphylococcus Aureus. *European Journal of Pharmaceutics and Biopharmaceutics* **2018**, *130*, 260–271.

45. Weldrick, P. J.; Hardman, M. J.; Paunov, V. N. Enhanced Clearing of Wound-Related Pathogenic Bacterial Biofilms Using Protease-Functionalized Antibiotic Nanocarriers. *ACS Appl. Mater. Interfaces* **2019**, *11* (47), 43902–43919.

46. Lankalapalli, S.; Kolapalli, V. R. M. Polyelectrolyte Complexes: A Review of Their Applicability in Drug Delivery Technology. *Indian Journal of Pharmaceutical Sciences* **2009**, *71* (5), 481.

47. Vicario-de-la-Torre, M.; Forcada, J. The Potential of Stimuli-Responsive Nanogels in Drug and Active Molecule Delivery for Targeted Therapy. *Gels* **2017**, *3* (2), 16.

48. Chen, Z.; Wang, Z.; Ren, J.; Qu, X. Enzyme Mimicry for Combating Bacteria and Biofilms. *Acc. Chem. Res.* **2018**, *51* (3), 789–799.

49. Al-Obaidy, S. S.; Halbus, A. F.; Greenway, G. M.; Paunov, V. N. Boosting the Antimicrobial Action of Vancomycin Formulated in Shellac Nanoparticles of Dual-Surface Functionality. *J. Mater. Chem. B* **2019**, *7* (19), 3119–3133.

50. Zhang, Y.; Zhang, H.; Zou, Q.; Xing, R.; Jiao, T.; Yan, X. An Injectable Dipeptide–Fullerene Supramolecular Hydrogel for Photodynamic Antibacterial Therapy. *J. Mater. Chem. B* **2018**, *6* (44), 7335–7342.

51. Al-Obaidy, S. S. M.; Greenway, G. M.; Paunov, V. N. Dual-Functionalised Shellac Nanocarriers Give a Super-Boost of the Antimicrobial Action of Berberine. *Nanoscale Adv.* **2019**, *1* (2), 858–872.

52. Al-Obaidy, S. S.; Greenway, G. M.; Paunov, V. N. Enhanced Antimicrobial Action of Chlorhexidine Loaded in Shellac Nanoparticles with Cationic Surface Functionality. *Pharmaceutics* **2021**, *13* (9), 1389.

53. Leick, S.; Kott, M.; Degen, P.; Henning, S.; Pasler, T.; Suter, D.; Rehage, H. Mechanical properties of liquid-filled shellac composite capsules. *Phys. Chem. Chem. Phys.* **2011**, *13*, 2765–2773.

54. Okur, M. E.; Karantas, I. D.; Şenyiğit, Z.; Üstündağ Okur, N.; Siafaka, P. I. Recent Trends on Wound Management: New Therapeutic Choices Based on Polymeric Carriers. *Asian J. Pharm. Sci.* **2020**, *15* (6), 661–684.